A SEISMIC REFRACTION SURVEY ALONG

THE SOUTHERN ROCKY MOUNTAIN TRENCH

by

GEOFFREY TAYLOR BENNETT

B.Eng., Royal Military College of Canada, 1971

A THESIS SUBMITTED IN PARTIAL FULFILMENT OF

THE REQUIREMENTS FOR THE DEGREE OF

MASTER OF SCIENCE

in the Department

of

GEOPHYSICS and ASTRONOMY

We accept this thesis as conforming to the
required standard

THE UNIVERSITY OF BRITISH COLUMBIA

October, 1973

In presenting this thesis in partial fulfilment of the requirements for

an advanced degree at the University of British Columbia, I agree that

the Library shall make it freely available for reference and study.

I further agree that permission for extensive copying of this thesis

for scholarly purposes may be granted by the Head of my Department or

by his representatives. It is understood that copying or publication

of this thesis for financial gain shall not be allowed without my

written permission.

Department of ___Geophysics & Astronomy___

The University of British Columbia
Vancouver 8, Canada

Date___October 13, 1973___

ABSTRACT

Deducing the structure and origin of the Rocky Mountain Trench has proven to be a difficult problem in the past. To understand this feature more fully and to obtain information about the entire crustal section, an unreversed seismic refraction profile has been recorded in the southern Rocky Mountain Trench from 50^ON to 53^ON. Using blasts from two open pit coal mines, forty-four useful recordings were obtained over a distance of 540 km. Three components of short period ground motion were recorded by tape recording systems; the vertical component was also recorded by elements of the Mica array.

Careful attention to amplitude scale factors results in the formation of a record section in which the energy pattern varies uniformly along the profile. A geometric ray theory interpretation involving Weichert-Herglotz integration of p-delta curves is used to obtain a velocity-depth structure. Approximate synthetic seismograms are then calculated using modified ray theory.

Refractors with apparent P-wave velocities of 6.5 - 6.6 km/s and 8.22 ± 0.04 km/s are interpreted as the surface of the Precambrian basement and the Moho discontinuity, respectively. A velocity gradient is present in the lower crustal section. The depth to basement beneath the western Rocky Mountains at $50^O30'$N is calculated to be 6.5 ± 1 km. Near Radium, a significant anomaly in the seismic data is best interpreted as a northeasterly-trending normal fault with a downthrow of 5.6 ± 1 km to the northwest. The directions are inferred from gravity and magnetic trends in the region. Alternatively, the anomaly could represent a disappearance of the basement surface west of the east wall of the Trench.

An anomalously thick crustal section is inferred from the data. A preferred model gives a depth of 51 ± 2 km southeast of Radium and 58 ± 2 km to the northwest. Study of a converted phase leads to the conclusion that there may be a discontinuity on the Moho surface beneath the Trench near 52^ON. Analysis of arrivals shortly after the P_n phase is consistent with the interpretation of a low velocity zone, approximately 7 km thick, 8 km beneath the Moho.

TABLE OF CONTENTS

LIST OF TABLES

LIST OF FIGURES

ACKNOWLEDGEMENTS

INTRODUCTION

The Rocky Mountain Trench is a long, narrow, intermontane valley bordering the west flank of the Canadian Rocky Mountains. As a subject of geologic controversy it is almost without peer, and much speculation has been directed towards its origin and underlying structure. An understanding of its deep structure would not only be important in itself, but would also yield valuable information about the formation of the entire eastern Cordilleran system.

Relatively few geophysical profiles have shed any light on deep crustal structure in this region. Seismic refraction studies have generally concentrated on the western Cordillera or the Interior Platform of Alberta; analyses of gravity data across the Trench have only pertained to the region south of $51^{\circ}N$; magnetic data have mainly been useful in determining the lateral structure only.
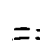
Subsequently, it has been discovered that large blasts from open pit coal mines near Sparwood (Figure 1) are regularly recorded on standard seismic stations. Using these blasts as good inexpensive sources of seismic energy, it was decided to run an unreversed seismic refraction profile northwest along the southern Rocky Mountain Trench.

Geophysicists from the University of B.C. performed the necessary field work during the summers of 1972 and 1973, recording a detailed profile along the Trench from $50^{\circ}N$ to $53^{\circ}N$. As the analysis in this thesis will show, the seismic data have led to new conclusions regarding crustal structure beneath the Rocky Mountain Trench.

Figure 1. The Southern Rocky Mountain Trench

Geologic setting and location of 1972-73
seismic recording sites
(inset after Douglas (1970))

Explanation of symbols:

△   portable seismic recording system
            (Kaiser shot only)
▲   portable seismic recording system
            (Kaiser and Fording shots)
Ⓜ   Mica array component
⊗   shot point
●   town

====   physiographic outline of Trench
—·—·—· provincial boundary
⌒⌒⌒ river
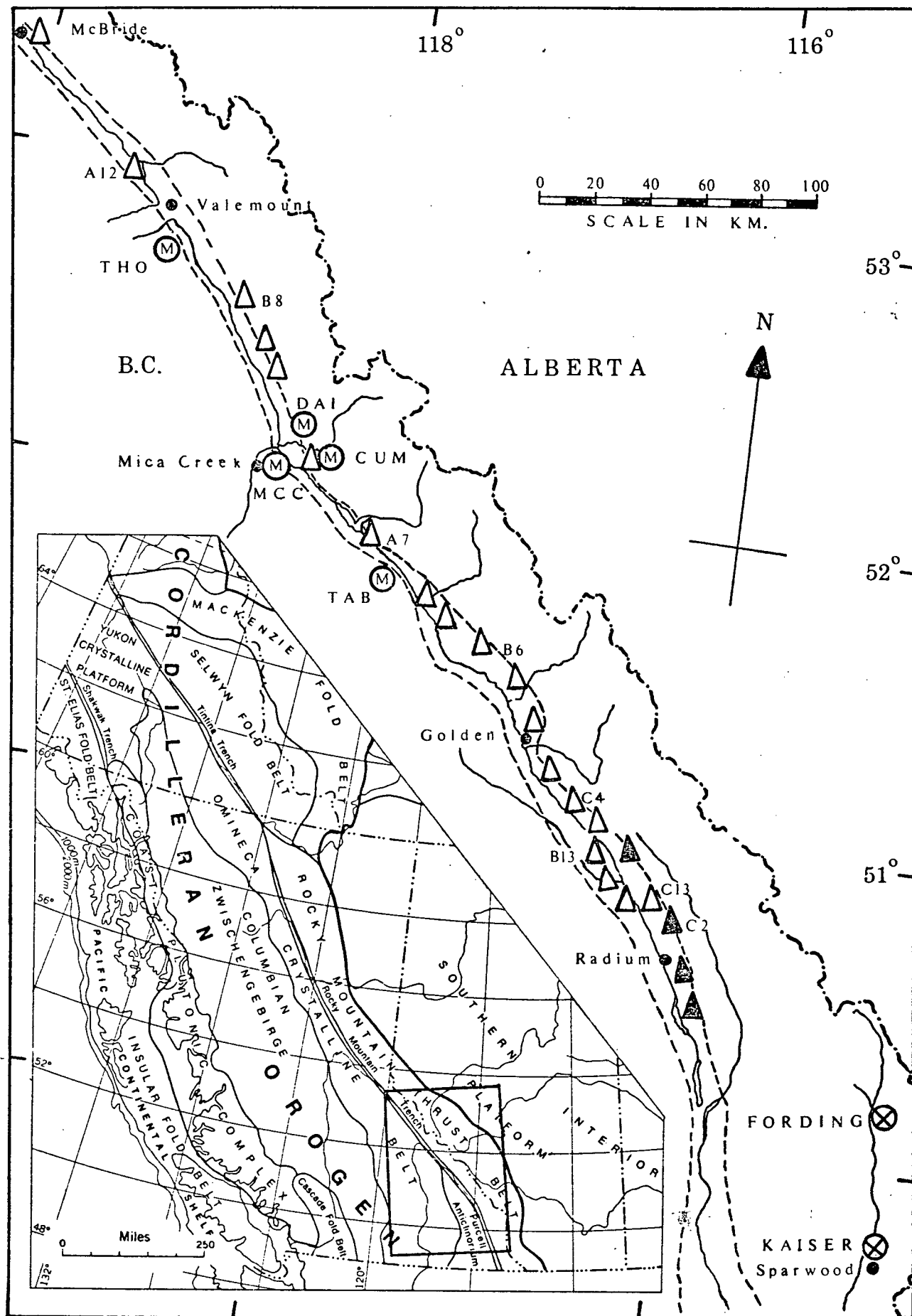
THE ROCKY MOUNTAIN TRENCH

General description

During the late 1850's, Palliser and Hector became the first men to remark openly on the "unbroken continuity" of the Trench, although their outlook was biased by the necessity of finding an easy route to the Thompson and Fraser Rivers (Schofield, 1921). In traversing the Trench near the international boundary, Dawson (1886) became the first geologist to recognize the "Columbia-Kootanie Valley" as "an orographic feature of the first importance." He was also the originator of what was to become one of the favourite preoccupations of Cordilleran geologists - speculation on the origin of the Rocky Mountain Trench.

As defined and named by Daly (1912), the Trench is a long, narrow, intermontane depression occupied by two or more streams alternately draining the depression in opposite directions. The Trench is long indeed, stretching over 1600 km from Montana to northern British Columbia (Figure 1). Its average strike is N 33° W, interrupted only at 55°N where the physiographic characteristics of the Trench fade into the Nechako plateau. In the south its trend is slightly sinuous, especially south of 50°N where the Trench widens to about 32 km (20 miles) as compared with an average width of 3 - 16 km (2 - 10 miles). It contains eight major rivers, separated by almost imperceptible gradients. Curiously, the local width of the Trench bears no relation to the size of the river occupying it. The elevation of the Trench floor varies only slightly from 2000 to 2700 feet above sea level along its entire length. Almost everywhere it is covered by a thick blanket of detritus - locally 1500 m (5000 feet) thick southwest of Sparwood (Lamb and Smith, 1962). On either side the walls rise to 900 - 1800 m (3000 - 6000 feet) above the floor, the eastern side generally being more precipitous than the more irregular western side.

These physical characteristics are striking enough, but the Trench is perhaps best known for its appearance as a lateral boundary between two radically different terranes to the southwest and northeast. Physiographically it marks the dividing line between the Rocky Mountains to the east and the Purcell, Selkirk, Monashee,

Cariboo, Omineca and Cassiar mountains to the west. Although the
Trench is parallel to the regional trend of the Rocky Mountain Thrust
Belt, individual ranges on both sides are slightly truncated (North and
Henderson, 1954).

Geologically, the contrast is even more apparent. The Rocky
Mountains have been formed exclusively from sedimentary miogeosynclinal
strata, predominantly carbonates and clastics. These layers have been
thrust to the northeast resulting in the well-known imbricate structure
of this mountain belt (Price and Mountjoy, 1970; Bally et al, 1966).
To many writers (Holland, 1959), the lack of intrusions and volcanic
activity in the Trench and to the east is remarkable. In marked
contrast, to the southwest lies the Omineca Crystalline Belt, a region
of highly metamorphosed intrusive granitic rocks. Deformation and
buoyant upwelling were initiated in this belt during the late Jurassic,
causing gravitational spreading to the east and subsequent formation
of the Rocky Mountain thrust sheets (Price and Mountjoy, 1970).

The boundary zone occupied by the Trench must continue to
greater depths since geophysical properties also show marked variations
across it. A study of magnetic anomalies over western Canada by
Haines et al (1971) shows two distinct zones in this area. East of
the Trench is the "Shield Zone", characterized by broad high amplitude
anomalies, striking north to northeast. To the west lies the "Cordilleran
Zone" showing long, narrow, northwest-trending anomalies. Geomagnetic
depth-sounding profiles have consistently found a transition from low I
to high I west to east across the Trench, where I is the vertical/hori-
zontal amplitude ratio of the local geomagnetic field (Caner et al, 1971;
Dragert, 1973). Using gravity data and noting the absence of a high
velocity layer in the lower crust under the western Cordillera,
Stacey (1973) has postulated a decrease in the density of the crust
and upper mantle to the west of the Trench. Further reference to some
of these studies will be made later.

Perhaps such geophysical anomalies point to a relatively
simple and unique origin for the Trench, but detailed geological
studies along its walls do not support such a conclusion. No "standard"
theory of erosion or structural control has found wide acceptance
along the entire length of the Trench, even though each idea is strongly
supported by evidence in different segments. Yet the unique continuity

and length of the Trench beg for a unifying interpretation, and it is
this fact which has spawned a fascinating literature in Cordilleran
studies.

The controversy

Dawson (1886) regarded the Trench as a strictly erosional
feature which formed subsequent to the uplift of the Rocky Mountains.
Daly (1912) enthusiastically called the Trench "unique among all the
mountain features of the globe for its remarkable persistence," and
attributed its origin to "a line of dislocation," perhaps a graben.
Several years later, Daly (1915) changed his opinion and offered an
alternative explanation as a zone of transcurrent faulting. His reason
was that the Trench does not have a typical symmetric graben structure.
Schofield (1921) returned to an erosional theory and described at
great length how ancient tributaries carved their paths through the
Trench to produce such odd features as the Big Bends of the Fraser
and Columbia Rivers. Even so, his theory is contingent upon tilting
and down-dropping of fault blocks within the Trench. South of Golden,
Shepard (1922) postulated thrust fault control and erosion along a zone
of weakness caused by the intersection of a large number of fault
planes. Finding westerly-dipping folds to the west and easterly-
dipping folds to the east, he also concluded that the Trench could
be a depression caused by this in-folding pattern. Later, Shepard (1926)
discounted Daly's graben structure completely and proposed, of all things,
a horst. Admitting this was unusual, he relied on long-continued
erosion to change the uplifted horst into a depression. Walker (1926)
and Evans (1933) also postulated thrust fault control along which
subsequent erosion could easily work, but discounted all theories of
transcurrent faulting and graben or horst structure. Without much
elaboration, Eardley (1947) linked the Trench to similar features in
the United States to produce a belt 3200 km (2000 miles) long,
presumably a rift zone. North and Henderson (1954) synthesized
previous theories, then devised a clever interpretation in which the
controlling faults originated as transcurrent faults but were later
converted into thrusts. And just when the question appeared to be
settled, Crickmay (1964) vehemently refuted these fault theories,
postulating an origin by the mere headward erosion of streams

in "a region inviting to trench-making." The importance of erosion
in forming the present physiographic outline is undeniable (Simony et al
(1972) found evidence for glaciation by an ice sheet 600 - 900 m
(2000 - 3000 feet) thick), but the lack of some form of structural
control is dubious, to say the least.

Leech (1959) suggested that the southern part of the Trench
has been formed by Cenozoic block faulting. This idea was substantiated
by Garland et al (1961), Thompson (1962), and J. Claig (oral communica-
tion, 1973). In addition, Gabrielse (1972) hypothesized block faulting
in the northern Trench following a period of transcurrent movement.

Detailed seismic reflection studies by Bally et al (1966)
favour a compatible idea that the Trench was formed after the main
thrusting phase of the Rockies by normal faulting along pre-existing
thrust plane surfaces. Dahlstrom (1970) and Price and Mountjoy (1970)
concur that low angle normal faulting could have occurred during periods
of relaxation following the compressive surges. Mudge (1970) found
that a similar interpretation in northwest Montana fitted the obser-
vations, although he hypothesized that the Trench is a "tear-away"
zone behind a region of gravity thrusting in the Rockies.

As Crickmay (1964) has stated, "...the existence of the
Rocky Mountain Trench is an enigma, a difficult and persistent puzzle
in geology....The origin of such valleys is thus a question that has
failed the best mental powers that have so far investigated it."
Although no final definitive solution to this enigma has appeared
(nor is it likely to), there remains one theory which is remarkably
persistent throughout the literature: "...that the Trench may mark
an old, deep fracture zone that has reasserted itself through the
allocthonous veneer" (Leech, 1965). This concept will be referred to
later in discussing the significance of the Rocky Mountain Trench
seismic data.

PREVIOUS GEOPHYSICAL STUDIES IN THE REGION OF THE TRENCH

Seismic refraction and reflection profiles

Within the Trench itself, only a very limited amount of previous seismic work has been carried out. Lamb and Smith (1962) ran a series of shallow reversed refraction profiles along and across the Trench at $49^{\circ}30'N$. A continuous refractor with a P-wave velocity of 5.2 - 5.5 km/s (17,000 - 18,000 ft/s) was mapped across the Trench and was interpreted as the Precambrian Purcell surface. This surface is exposed at 2500 - 3000 feet above sea level on the Trench margins and dips to 2000 feet below sea level in the centre. It is overlain by Cenozoic sediments with a P-wave velocity of 3.3 km/s (11,000 ft/s) and a thin "loose" layer in the centre of the Trench with a velocity of 2.5 km/s (7500 ft/s). Bally et al (1966) observed seismic reflections across the Trench near $49^{\circ}15'N$. Strong, "near-basement" arrivals beneath the Rocky Mountains were interpreted as reflections from just above the westward extension of the Precambrian shield. The Shield, comprised of metamorphic and igneous rocks and referred to as the crystalline "basement", appears to dip gently westward to the east wall of the Trench. Across the Trench, the data was noisy and showed no coherent reflections, but the extension of the basement reflection could be observed again beneath the Purcell mountains for a short distance on the western side. Despite the poor data, Bally et al (1966) assumed that the basement does exist beneath the Trench at this latitude at a depth of 8.5 ± 0.3 km (28,000 ± 1000 ft) with an over-lying layer of velocity 5.2 - 5.5 km/s.

To the east, seismic refraction studies by Cumming and Kanasewich (1966) have been extended and re-analysed by Chandra and Cumming (1972) to delineate the deep crustal structure beneath southern and central Alberta. Cumming and Kanasewich (1966) gave a depth to the Moho of 46 km beneath the Trench near $50^{\circ}30'N$, although how this figure was obtained is unclear. The more recent work by Chandra and Cumming (1972) has interpreted a partially reversed refraction profile along $50^{\circ}30'N$ from $118^{\circ}W$ to $108^{\circ}W$. An abrupt discontinuity in seismic velocities and refractor depths has been postulated beneath the Front Ranges of the Rocky Mountains. A constraint used in the interpretation of this section was the work of White et al (1968) in the Intermontane

Belt (Columbian Zwischengebirge in Figure 1), since that section of
the profile west of the Front Ranges was unreversed. The upper crustal
velocities found by White et al (1968) were assumed to extend to the
eastern margin of the Rocky Mountains. Integration with observed
Bouguer gravity anomalies has allowed a tentative velocity-depth model
beneath the Trench of 6.00 km/s from 0 - 20 km, 6.50 km/s from 20 - 31 km,
7.15 km/s from 31 - 49 km, underlain by the upper mantle with P-wave
velocity 8.20 km/s. It must be emphasized that this structure, except
for the P_n velocity, has been deduced by extrapolation of the eastern
profiles to fit data recorded in central British Columbia.

Data from seismic refraction surveys in British Columbia up
to 1966 were synthesized by White et al (1968). Signals from the 1958
Ripple Rock explosion in the Strait of Georgia near Vancouver were
recorded throughout eastern B.C. along latitude 51^ON. From this
unreversed profile, the data indicated a P_n velocity of 7.76 km/s and
an average crustal thickness of 31 km in the eastern Cordillera.
Subsequent northwest-striking profiles in the Intermontane Belt showed
a uniform upper crustal P-wave velocity of 6.1 km/s with the Moho
discontinuity dipping gently eastward at a rate which would produce
a 45 km crustal thickness immediately east of the Rockies. However,
this figure was extrapolated from a profile in southwestern B.C. and is
probably an over-simplification. Forsyth (1973) found a significant
800 km wavelength on the Moho which shows a rather strong easterly dip
in the Omineca Crystalline Belt. Using a reversed profile in the
vicinity of 53^ON, 122^OW, the Moho was observed to dip 10° to the east
with an average P_n velocity in the area of 8.06 km/s. One model for
this profile shows an upper crustal P-wave velocity of 5.6 km/s to
a depth of 3.5 km, a 6.2 km/s layer with a gradient to 30 km and a
7.5 km/s layer with a gradient to the Moho at 45 km. An alternate
model with no 7.5 km/s layer gives a crustal thickness of 35 km, and
was preferred since the evidence for this deep crustal layer is marginal.

Two long range unreversed profiles were run in a southeasterly
direction from Greenbush Lake (51^ON, 118^OW) in 1969 (Hales and Nation,
1973). The more westerly profile travels through the Omineca Crystalline
Belt into the U.S. and gives a model of 6.0 km/s to 22.6 km depth and
6.41 km/s to the Moho at 37.5 km depth. The P_n velocity is 8.04 km/s.
The more easterly profile, which crosses the Trench in northern Montana,

provides P_n information only (8.04 km/s) but the P_n branch intercept
is the same for both profiles (7.87 sec).

Gravity surveys

A small-scale survey by Garland et al (1961) found three
deep basins filled with unconsolidated material in the Trench south
of $49^\circ 30'N$. This discovery lent strong evidence to a theory of block
faulting in the Trench at this latitude.

On a much larger scale, Stacey (1973) has interpreted a
gravity profile across the Cordillera which includes the Trench from
$49^\circ N$ to $51^\circ N$. A gravity minimum of -200 mgal occurs over the northern
part of the Purcell Mountains and the adjacent Trench. In conjunction
with the rest of the data, this is interpreted as a decrease in the
density of the crust and upper mantle west of the Trench, with an
expected crustal thickness approaching 60 km beneath the Rocky Mountains.
However, if the crust is shown to be very much thinner than 60 km,
this density change must begin further east below the Rocky Mountains
themselves.

Magnetic surveys

Combining magnetotelluric and geomagnetic depth-sounding
data for the Cordillera, Caner et al (1971) concluded that the Cordillera
west of the Trench is underlain by a highly conductive layer starting
at a depth of 10 - 15 km with indefinite thickness of about 20 - 40 km.
The crustal layer has a sharply defined eastern margin where the I values
begin to increase to the east. This transition lies a few kilometers
to the east of McBride where it strikes N 30°-35° W, parallel to the
Trench. It continues as far south as Valemount and probably further
to the vicinity of $51^\circ 30'N$ after which it swings southward into an
almost north-south strike.

Interpreting a geomagnetic depth-sounding profile across
the Trench near Golden, Dragert (1973) concluded that the highly
conductive zone in the western region is probably at, or dips to a
depth of, about 40 - 50 km beneath the Rocky Mountain Trench transition
region. To agree with Caner et al (1971), this model requires an
eastward dip under the Rocky Mountain area of approximately 6°-11°.

Most of these geophysical findings are directly relevant
to an interpretation of the Rocky Mountain Trench seismic data.
In the light of this latest evidence, a number of these profiles will
be discussed further in a subsequent section.

COLLECTION OF DATA

Seismic instrumentation

Recording systems used in the Rocky Mountain Trench project are illustrated schematically in Figures 2a, 2b and 2c. The shot point system was very simple and consisted of a two-channel chart recording of the WWVB time signal and the output of a geophone planted near the blast.

Three portable seismic recording systems, designated A, B and C, were in use throughout the project. Each recorded three components of short period ground motion onto FM tape (Figure 2b). Both low and high level amplifier outputs were recorded so that amplitude information would be preserved in the event of a signal voltage overload. Also recorded on tape were one or two time signals, depending upon the quality of reception. The WWV time signal was used to trigger a timing unit which then sent minute and second marks to tape; output from the WWVB receiver was recorded directly. The WWVB signal was generally preferred when obtainable, in order to improve the accuracy of traveltime calculations. One annoying problem throughout the project was the occurrence of 6 Hz noise on the amplifier channels of system C (Figure 5b). Eventually the problem was traced to induction effects of the timing unit on the amplifier inputs, but was not satisfactorily resolved until near the end of the project. Less serious electronic noise occurred sporadically in systems A and B, sometimes necessitating the use of a third battery.

The Mica telemetered seismic array was operating by the fall of 1972 in the configuration shown in Figure 2c. It should be noted that the data obtained from this array were equivalent in most respects to that recorded by the portable systems. Tape recorder specifications, amplifier filter cutoffs and timing were the same, although the resonant frequencies of the Mica seismometers were slightly higher at 1.63 Hz, and only the vertical component of ground motion was recorded. A detailed description of this array has been given elsewhere (Ellis and Russell, 1972) and will not be repeated here. Four of the seismic sites are located on peaks above the Rocky Mountain Trench (Mount Thompson (THO), Mount Dainard (DAI), Mount Cummins (CUM), and Tabernacle Mountain (TAB): see Figure 1); one other site (MCC) is located near the recording station
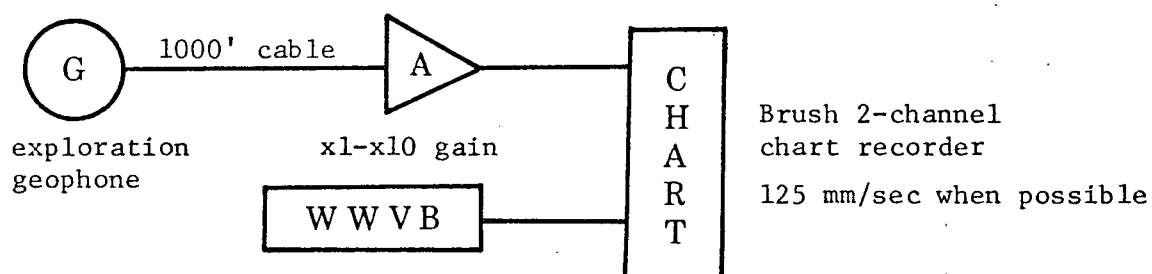
Figure 2a. Shot point recording system
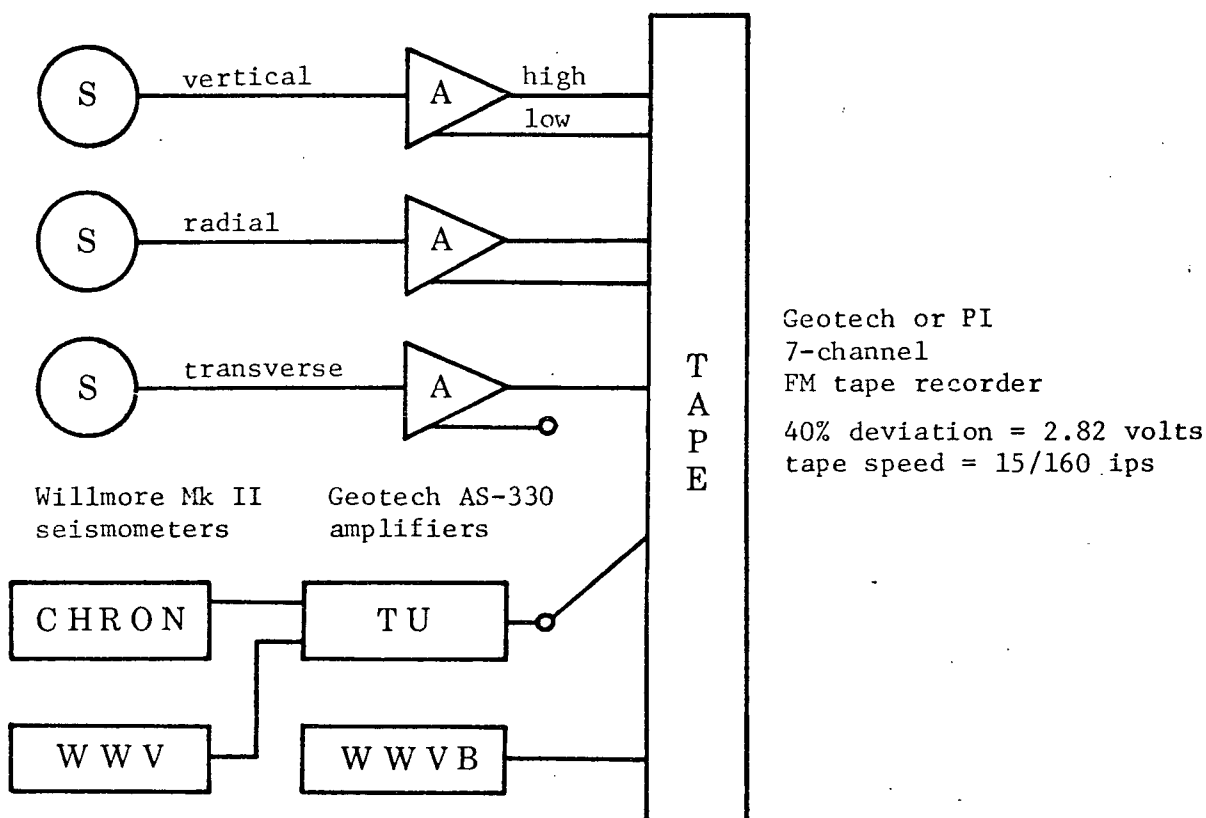
Figure 2b. Typical 3-component portable seismic recording system

Seismometer natural frequency adjusted to 1 hz.

Amplifier low output is attenuated from 70 db in 6 db steps. High output separation is 18,24, or 30 db above low output. Filter cutoffs set at 0.75-12.5 hz.

UBC timing unit outputs second and minute marks, electronically triggered from WWV receiver and controlled by 60 hz output of chronometer.

THO

DAI

CUM

TAB

Willmore Mk I
seismometers
(vertical only)

Geotech 42.21
telemetry amplifiers

Geotech 46.11
FM discriminators

D

PA

Σ

TAPE

MCC

S

A

Geotech EA-310
amplifiers

PA

WWVB
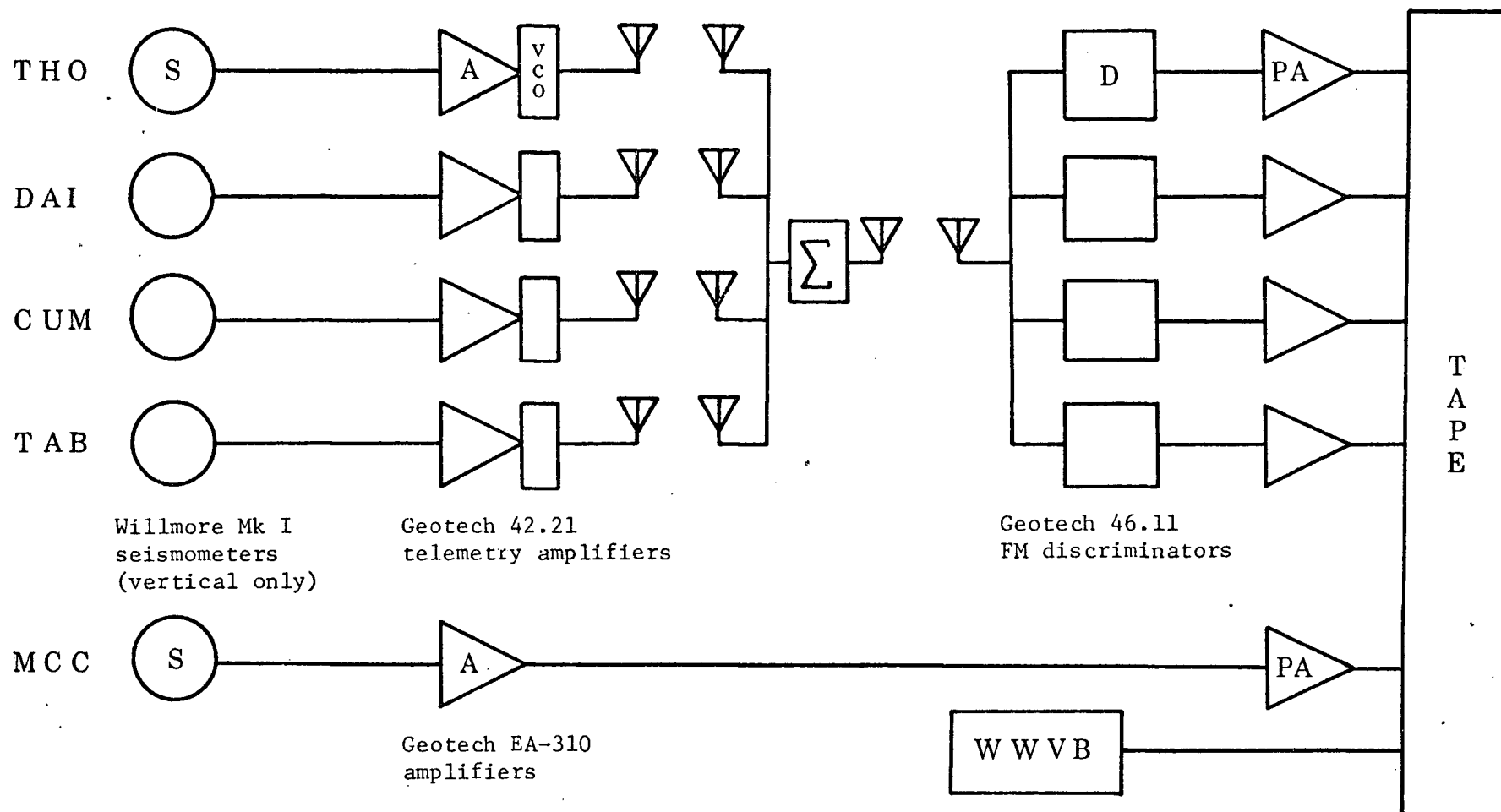
Figure 2c.   Mica Creek telemetered seismic array

Seismometer natural frequency adjusted to 1.63 Hz.

Telemetry amplifiers have 100 db maximum gain; post-amplifiers raise signal level
  by an additional 0,6, or 12 db. Filter cutoffs approximately 1-12.5 Hz.

Geotech or PI 7-channel FM tape recorder; 40% deviation = 2.82 volts;
  tape speed = 15/160 ips.

at Mica Creek and is operated by the Earth Physics Branch. However, its inferior signal-to-noise ratio made it of little use to this project. Five shots recorded by this array in February and June, 1973 were utilized in this study.

Following the 1972 field season the systems were calibrated in the same configuration as the operating mode, except that the tape recorder was disconnected. The calibration technique involved the use of the Maxwell bridge and current source analysis of Kollar and Russell (1966). Graphs of acceleration, velocity and displacement sensitivity were drawn for each of the nine seismometer/amplifier systems; a typical velocity sensitivity curve as used in later calculations of scale factors is shown in Figure 3. The tape recorder response was essentially flat up to 17 Hz and thus did not affect the total system response in the region of interest. Following the 1973 field season the same systems were "spot" calibrated and were found to have deviated by less than 1%. Calibrations of the Mica array were performed by R.D. Meldrum before the system was installed, and a computer program was used to determine the total system response. In the field, two types of transient calibrations were performed on systems A, B and C as an operational check, but were not used in subsequent analysis. The "K" test described the seismometer response to a voltage step input, while the "S" test described the response of the complete seismometer/amplifier system.

Field methods

The normal procedure in the field was to have one member of the party record the time of detonation at the shot point, while three portable systems were taken to predetermined locations along the Trench to the northwest. Horizontal seismometers were aligned in radial and transverse directions to the shot. Communication between shot and receiver was by radio telephone, thus greatly eliminating problems caused by shot cancellations, delays, equipment malfunctions, etc. Large blasts were recorded from the Kaiser Resources open pit coal mine near Sparwood and the Fording Coal Ltd. open pit operations 50 km to the north. As is apparent from Figure 1, both shot points are approximately on strike with the Trench, with recorded seismic energy actually entering the Trench zone in the vicinity of Radium. An unexpected feature of these blasts is that, despite the large charge size (see Table I),
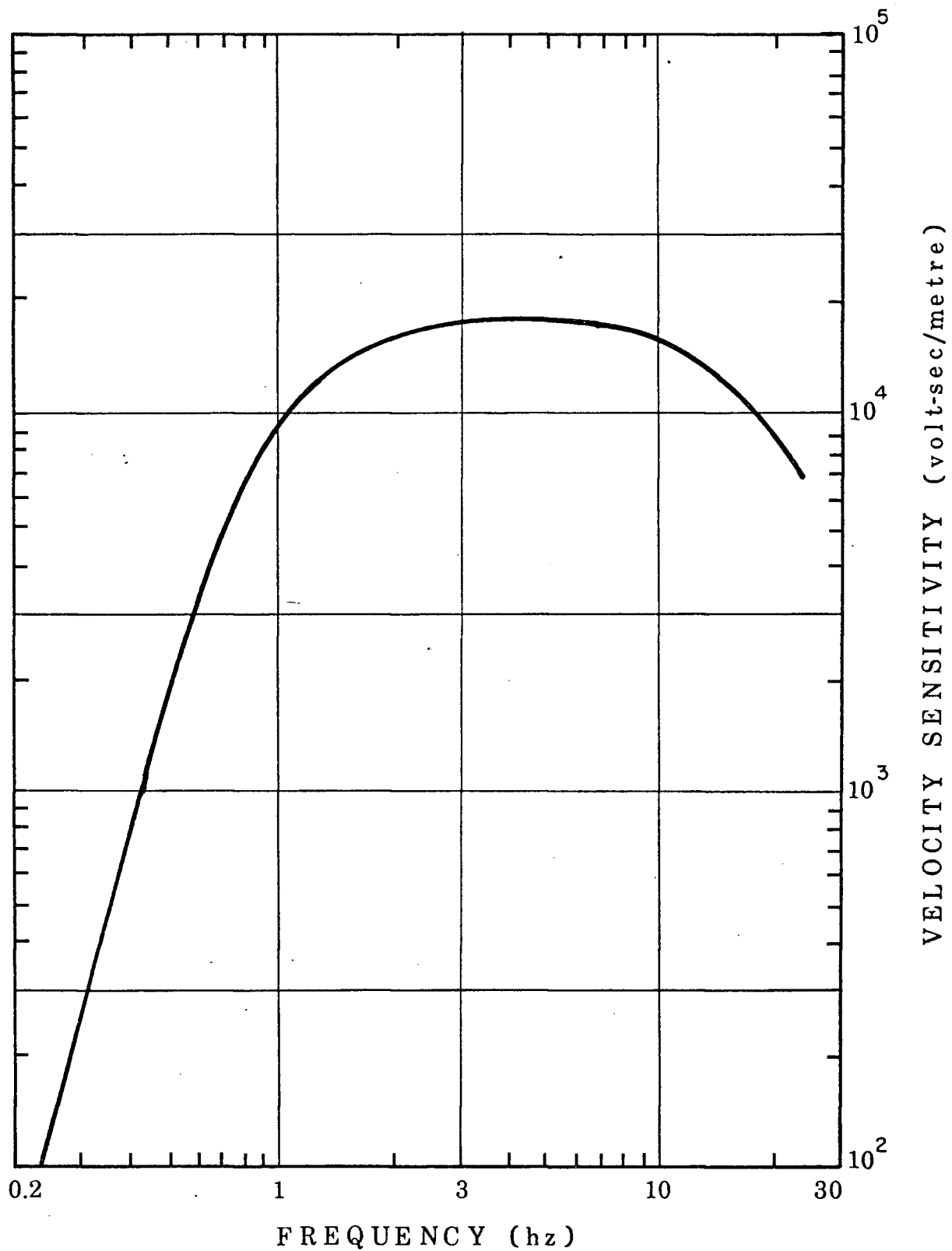
Figure 3. Typical velocity sensitivity curve for Willmore Mk II seismometer
and AS-330 amplifier with -3 db points of filter set at 0.75, 12.5 Hz.
Low output response at 24 db attenuation.
Tape recorder response not included.

SHOT POINT LOCATIONS ROCKY MOUNTAIN TRENCH SEISMIC PROJECT 1972 - 1973

Shot Number	Date	Mine and Pit	Charge size (lbs.)	Latitude (deg min)	Longitude (deg min)	Origin (h	Time m	(U. T.) s)
1	June 8	Kaiser	not useable				not obtained	
2	June 23	Kaiser-Harmer 1	∿300,000	49°46.72'	-114°49.83'	18	22	34.20 ± .14
3	June 23	Fording	∿ 60,000	50°12.32'	-114°51.67'	22	18	00.74 ± .02
4	June 24	Kaiser-Addit 29	∿300,000	49°45.16'	-114°48.50'	18	15	23.07 ± .03
5	July 7	Kaiser-Harmer 11	∿400,000	49°47.46'	-114°50.09'	20	00	58.86 ± .02
6	July 8	Kaiser-Harmer 1	∿250,000	49°46.77'	-114°49.85'	18	16	06.11 ± .02
7	July 19	Kaiser-Addit 29	∿366,000	49°45.57'	-114°48.75'	19	29	50.49 ± .02
8	July 21	Kaiser-Harmer 11	∿600,000	49°47.39'	-114°50.16'	19	29	34.68 ± .03
9	Feb 22/73	Kaiser-Addit 29	∿400,000	49°45.30'	-114°48.65'	19	13	17.91 ± .02
10	Feb 23	Kaiser-Harmer 11	∿500,000	49°47.32'	-114°50.15'	20	59	06.07 ± .02
11[1]	June 20	Fording	∿400,000	50°12.28'	-114°51.65'	18	36	50.69 ± .05
12[2]	June 20	Kaiser-Harmer 1	∿300,000	49°46.75'	-114°49.84'	18 / 19	36 / 55	50.96 ± .03 / 20.52 ± .03
13	June 21	Kaiser-Harmer 11	∿300,000	49°47.46'	-114°50.00'	18	14	29.88 ± .02

Notes: [1] First origin time represents initial detonation of a smaller charge; second origin time represents detonation of a larger charge in a different part of the pit; the distance between blasts is ∿1,000 ft.

[2] No shot point recording. Location is given by the average of all other Harmer 1 blasts. Time is based on P_n arrivals at Mica array, the latter being calibrated by earlier blasts.

Typical blast area: (200 to 300 ft by 600 to 900 ft)

Shot point location calculated for center of blast area specified to nearest 100 ft. The associated errors in the coordinates are:

Latitude ± 0.02'
Longitude ± 0.03'

Table I. Shot point data.

first arrival seismic energy was very weak beyond about 400 km and was only recorded by virtue of the excellent signal-to-noise ratio of the Mica array. This lack of efficiency is probably due to the "ripple-fire" technique in which a pattern of shots is laid out with up to several milliseconds delay between each detonation. However, this loss of compressional energy is compensated by strong shear wave generation and indeed, large S-wave arrivals appear later on all the records, even for shots with very little delay. This is an important aspect of the profile and will be utilized in future studies to deduce a structure based on the integrated P- and S-wave data.

Shots were numbered chronologically (Table I) and appended to the system name to designate records. (Thus, B6 is the recording of shot 6 by system B; DA10 is the recording of shot 10 at Mount Dainard.) Some locations (A2 and A3, B2 and B3, C2 and C3, B11 and B12) recorded blasts from both shot points (see the shaded triangles in Figure 1), while the Mica array recorded signals from shots 9 to 13. The profile itself extended from site B2/B3 southeast of Radium (84 km from Fording, 112 km from Kaiser) to site A13 near McBride (539 km from Kaiser). On the profile just north of Radium a clustering of sites can be seen. After the initial survey was completed in 1972, anomalous traveltime behaviour was observed in this region, resulting in the addition of four sites to this locality in 1973. All field sites in the project lay near the east wall of the Trench, except for B4, C12 and B13 which lay on hills in the centre. Although attempts were made to locate sites on bedrock wherever possible, the nature of the Trench made this task difficult. Consequently, many sites probably were underlain by several hundred feet of unconsolidated sediments.

Shots from Fording turned out to be useful only with the A3 and B3 recordings south of Radium. Excessive timing noise in system C obliterated C3; B11 was very weak and emergent, and coda from an earlier blast interfered with the arrival of shot 11 at the Mica stations. Table I indicates another problem with shot 11. Two shots were detonated, the larger one being delayed by about 0.3 sec from the first. The decision was made to use the earlier origin time, although its associated energy was less.

Record B7 (north of DAI) was obliterated by river noise and system malfunctions. Record C7 (beside CUM) recorded horizontal

components of ground motion only, while B6, B11, B12, B13, C12, and C13 recorded only the vertical and radial components. The Mica array, of course, recorded the vertical component only.

PRELIMINARY DATA ANALYSIS

Digitization

After the data had been recorded on FM magnetic tape,
digitization was performed in the Department of Geophysics and Astronomy
Laboratory. The procedure can be described briefly as follows.
The recorded signal is played back on a Sanborn 3907B FM tape recorder
and is fed into a Scientific Data Systems A/D converter. Sample-and-hold
amplifiers in the converter allow simultaneous digitization of four data
channels. The converter itself receives instructions from an Interdata
Model 4 computer which is tied to a Teletype terminal. The digitized
signal is then dumped onto seven track magnetic tape. The digitizing
interval is controlled by a clocking system which triggers the A/D
converter. To ensure a faithful reproduction of the analog signal in the
time domain, a digitizing interval of 85 Hz (0.012 sec) was chosen.
Therefore, since the Nyquist frequency of the digitized data was 42.5 Hz
and the high cutoff of the AS-330 amplifiers was 12.5 Hz, any aliasing
problems were completely eliminated. After digitizing, the data were
demultiplexed and written on nine track tape in blocks 11 - 12 seconds
long for analysis on the U.B.C. IBM 360/67 computer. Minor tape speed
variations between the systems were successfully accounted for in the
plotting programs, resulting in a maximum timing error of 0.005 sec
at each point. The analog tape records were later spliced onto a single
reel and stored as a backup.

Filtering

Although many of the records showed excellent signal-to-noise
ratios, a substantial number required bandpass filtering. For these
records power spectra of the background noise prior to onset and of the
first several seconds of P coda were calculated. A comparison between
the two spectra for each record then gave an indication of the most
effective bandpass limits. A clear example of this method is shown in
Figure 4a. The site at A3 was plagued by large amplitude monochromatic
5 Hz noise which effectively disguised the seismic energy from a Fording
shot (Figure 5a). However, the power spectrum of the arrival showed
considerable energy in the 6 - 8 Hz range, so that a bandpass filter from

Figure 4a. Comparison of power spectra for pre-arrival noise and for the seismic signal at A3.
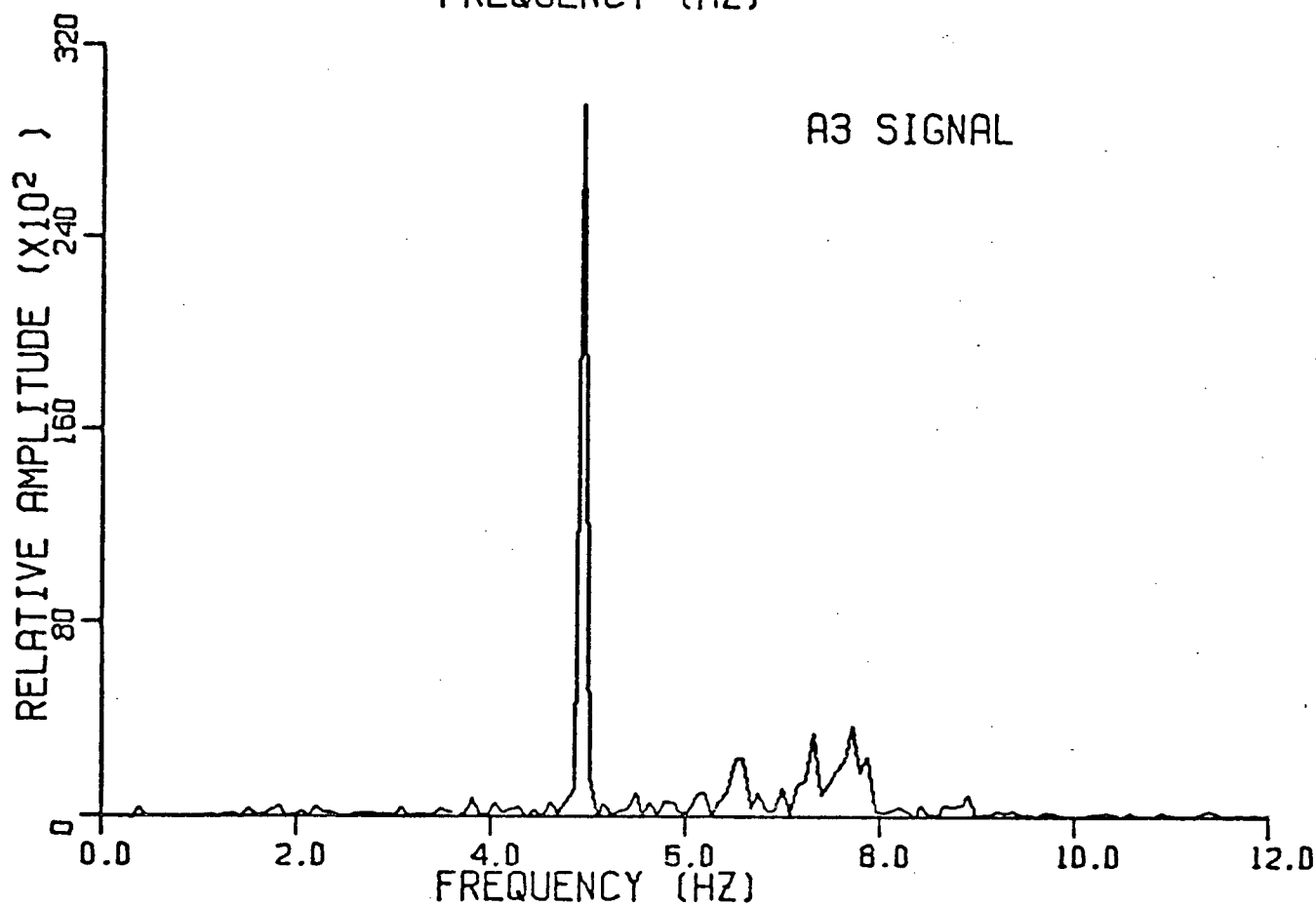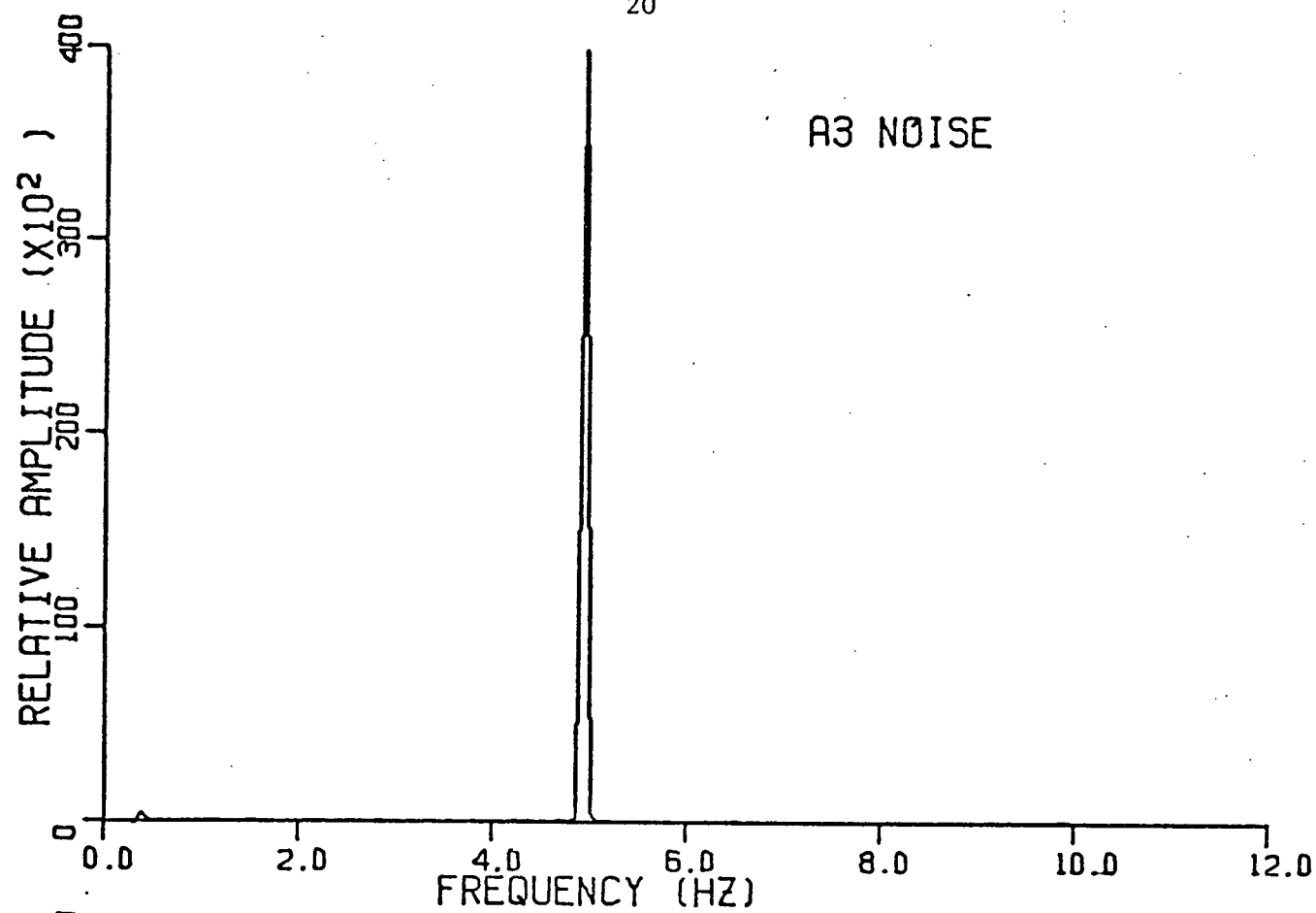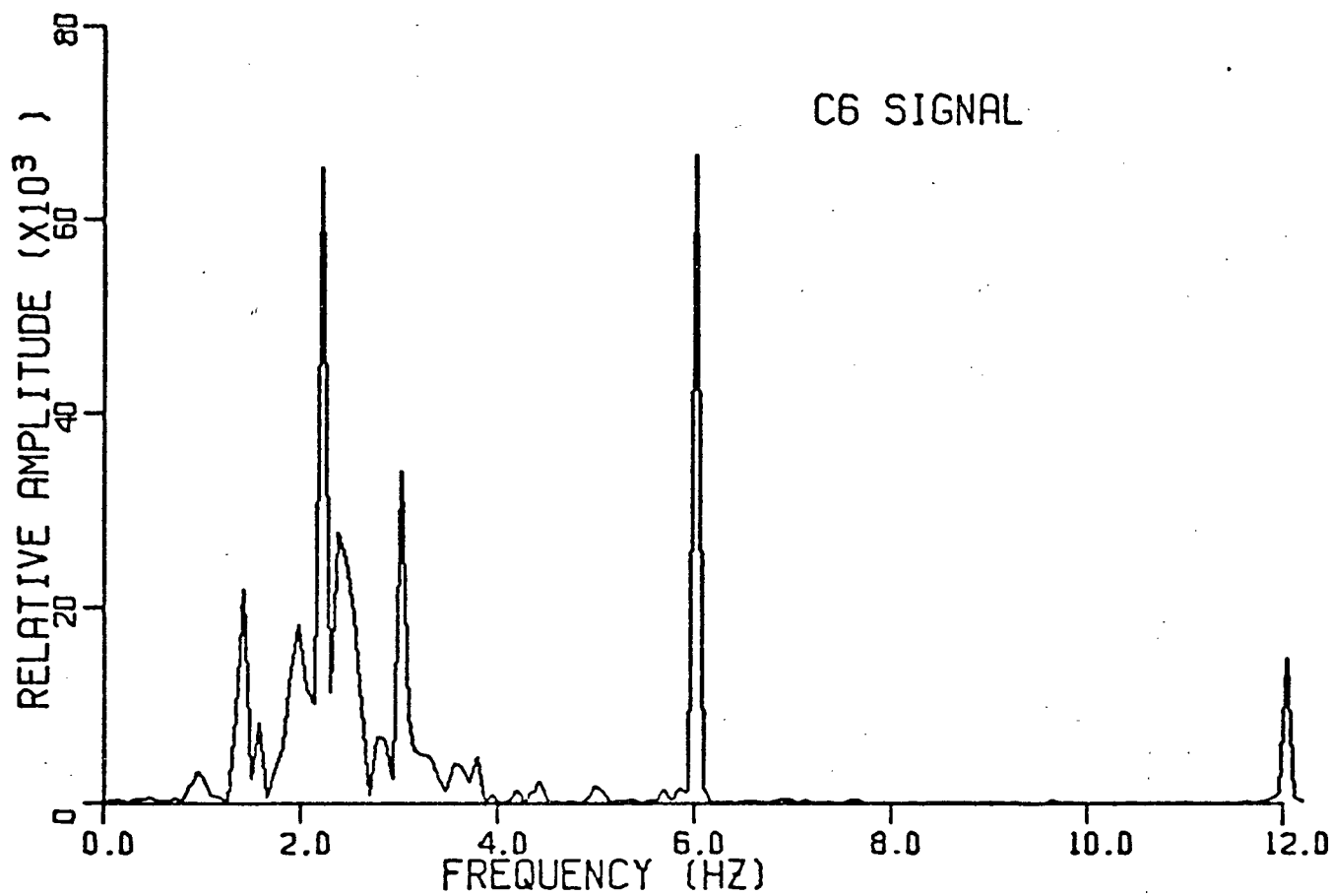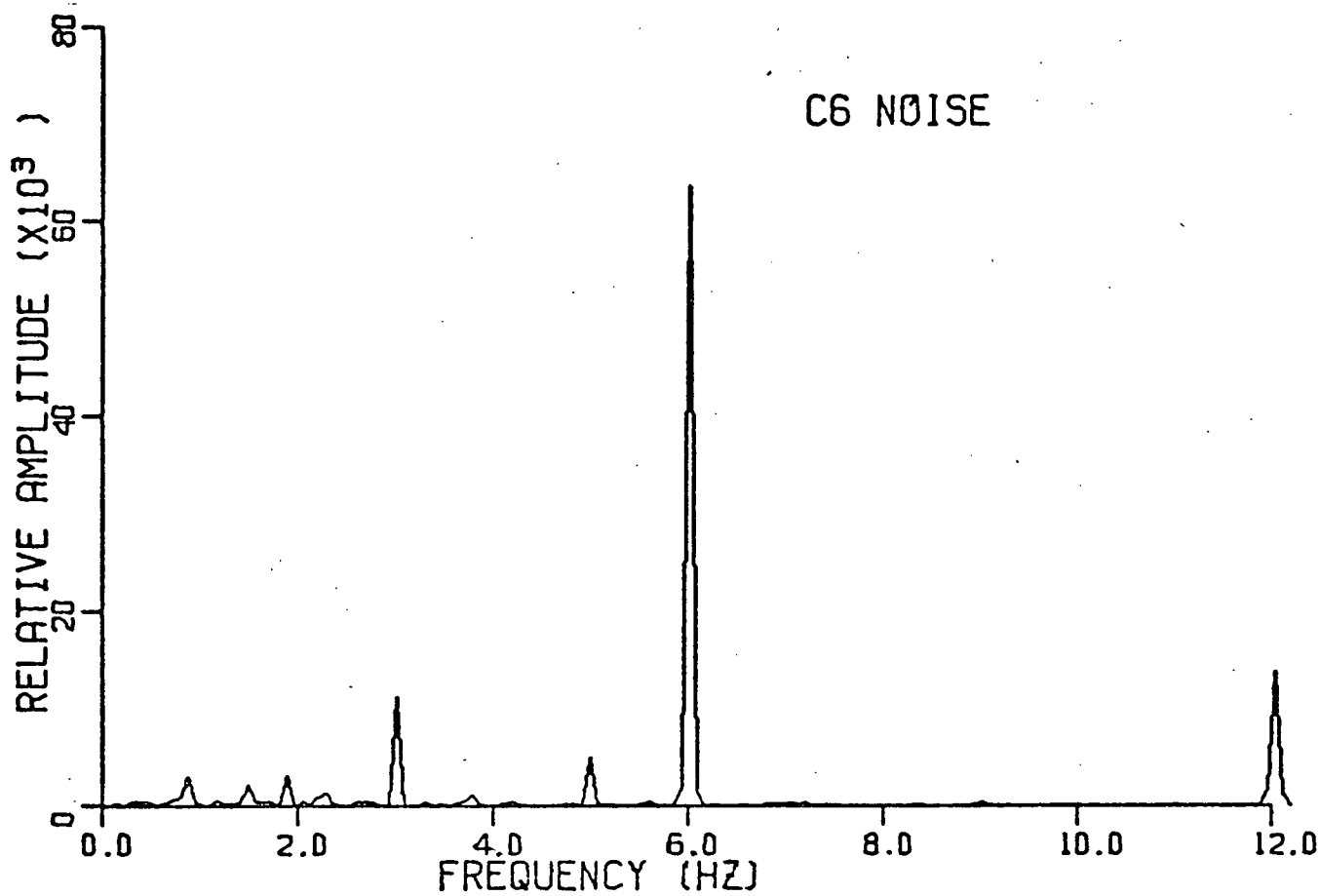
Figure 4b. Comparison of power spectra for pre-arrival noise and for the seismic signal at C6.

A3 UNFILTERED
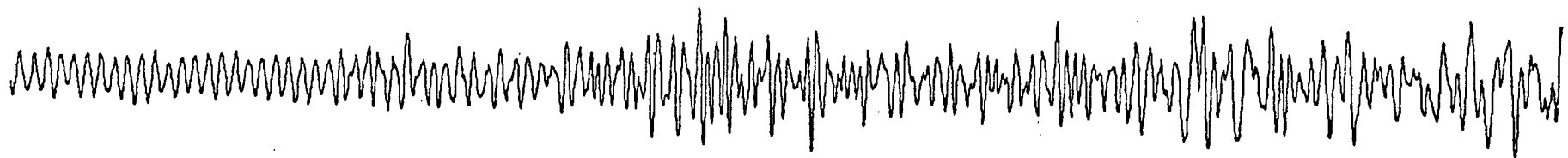
1 SEC.

FILTERED: 5.7- 11.8 HZ

Figure 5a.   Seismic signal at A3 before and after application of Butterworth band-pass filter.

C6   UNFILTERED

FILTERED: 0.2 - 4.4 HZ

1 SEC.
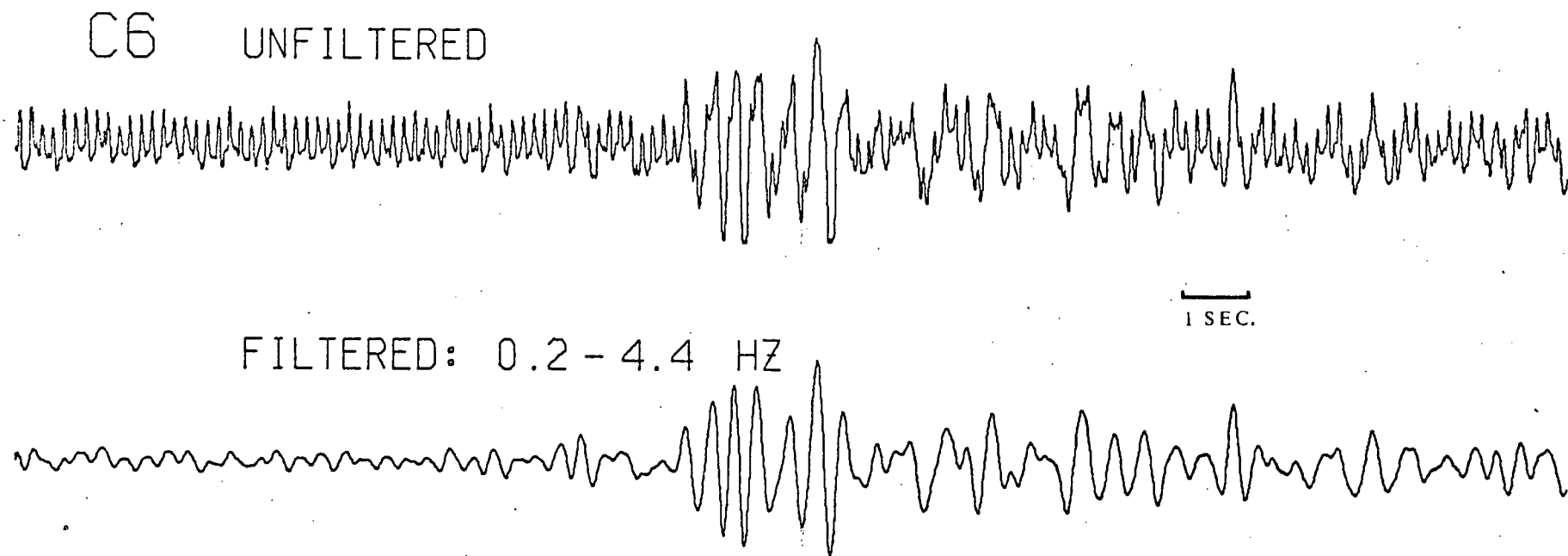
Figure 5b.   Seismic signal at C6 before and after application of Butterworth band-pass filter.

5.7 - 11.8 Hz eliminated most of the unwanted noise (Figure 5a).

A fourth order Butterworth bandpass filter was used throughout, and can be described by the following relation (Kanasewich, 1974):

$$|Y(\Omega)|^2 = (1 + \Omega^{2n})^{-1}$$

where $\Omega = \dfrac{\omega^2 - \omega_1\omega_2}{\omega(\omega_2 - \omega_1)}$ is a normalized frequency

$Y(\Omega)$ is the transfer function

ω_1, ω_2 are the low and high frequency cutoffs

$n = 4$

The data are convolved with the impulse response of the filter, then reversed and passed through the same filter again. This is in order to achieve zero phase shift in the filtered signal. The resulting filter response is down by 6 db at the cutoff frequencies. Thus, care had to be taken in the filtering process not to attenuate signal frequencies which were juxtaposed with the undesirable noise.

Butterworth filtering was used also to eliminate much of the system C timing noise which occurred on records from shots 2 to 6. The power spectra of C6 background noise (Figure 4b) shows 3 Hz noise with a pronounced harmonic at 6 Hz and one at 12 Hz. The signal spectrum shows a predominance of energy in the 1 - 4 Hz range, dictating the use of a 0.2 - 4.4 Hz filter as shown in Figure 5b. The signal is definitely enhanced, but 3 Hz noise is still present and cannot be removed by bandpass filtering. Noting that this timing noise appears to be in phase across all three seismic channels, a simple technique was attempted in which the trace of one seismometer, prior to the onset of seismic energy, was physically subtracted from another. It was hoped that this would at least delineate the first arrival, but the noise apparently is not as regular across the three channels as it appears to the eye. However, this technique may be worth additional effort.

Formation of record sections

In order to form record sections, calculations of traveltimes, distances and amplitude scale factors were necessary. Shot times from the shot point records were corrected for the blast-to-geophone distance and the difference between WWVB coded time and Universal Time (UT),

giving an origin time with an error of 20 -. 30 msec (Table I).
Traveltimes were calculated using plots of the demultiplexed data
blocks and WWVB/UT corrections were added. In addition, elevation
corrections were made to bring all recording sites to a 2000 feet
above sea level datum, the approximate elevation of the Trench floor.
The resulting correction was quite small, the maximum change in
traveltimes being only 0.15 sec. Shot locations were calculated by the
mining engineers from a mine grid tied to nearby bench marks. The assoc-
iated errors are 0.02' latitude and 0.03' longitude. Using aerial
photographs and 1:50,000 scale topographic maps, site locations
generally were determined to a similar accuracy (approximately 40 - 50 m).
Distances were calculated using a pre-existing program giving final errors
in the order of 0.1 km.

Amplitude scale factors were deemed a very necessary factor
as shown by Forsyth (1973). Digitization factors were constant, but
amplifier settings, signal frequencies, system responses, shot energies
and distances were not. From the power spectra analysis, it was observed
that the seismic energy in all records except those from shot 3 fell
in a narrow frequency band from 2 - 4 Hz. Records B3 and A3 showed
energy in the 6 - 8 Hz range (Figures 4a, 4b). Therefore, since the
signal frequencies are higher than the low cutoff frequency, it can
be assumed that the seismometers recorded ground velocity (Figure 3).
Nevertheless, this is only an approximation near the low cutoff.
Values of velocity sensitivity were then picked from Figure 3 to coincide
with the predominant signal frequencies recorded by the particular system.
Once corrected for amplifier settings, this value became the initial
amplitude factor.

It is an established fact (e.g. Forsyth, 1973; Berry and
Fuchs, 1973) that energy yield from a blast bears little relation to
the charge size. Accordingly, amplitudes of each shot were picked from
short-period photographic records recorded at the standard stations
PNT and SES, and an average of the two values was then used as the shot
factor. It was subsequently observed, for example, that although
shot 4 was of slightly less than average size, it produced by far the
largest amplitudes.

Finally, it was decided to introduce a factor to account for
geometrical spreading of the seismic energy along the profile.

Since the weak P_n arrivals at the far end of the profile are the most severely affected by spreading, a factor inversely·proportional to the head wave coefficient was applied to the data. Cerveny and Ravindra (1971, p. 147) show that at large epicentral distances (r), and other factors being constant, this coefficient is approximately proportional to $1/r^2$. Therefore, the data were multiplied by a factor of r^2 to enhance the head wave arrivals, although this factor tends to over-emphasize body waves which attenuate with distance by a factor of $1/r$.

After normalizing with respect to the largest observable amplitude, the traces were consolidated in the form of record sections. When these amplitude factors are combined, it is intended that the resulting energy pattern varies uniformly across the profile and that amplitude anomalies in the record section are significant in terms of underlying structure.

INTERPRETATION

General features of the record section

The normalized record sections, reduced by an average crustal velocity of 6.5 km/s, are shown in Figures 6 and 7. Figure 6 has been corrected for all amplitude factors except that for geometrical spreading, whereas amplitudes in Figure 7 have been multiplied by the square of the distance. Even though the overall amplitude correction factors at different sites vary by over two orders of magnitude, a smooth variation of energy with distance resulted.

One exception to this pattern occurred in the centre of the section where records A6, B6 and C6 had amplitudes seemingly too large by at least a factor of three. However, upon examining the firing pattern of shot 6, it was discovered that the shots were detonated along the perimeter of a narrow, approximately elliptical shape, with long axis pointing north. Therefore, it is quite possible that the radiation pattern would show significant differences between the east-west directions of SES and PNT and the southeast-northwest direction of the profile, and that the amplitudes of incident energy would not be the same. Since seismograms from a standard U.S. station to the southeast were unavailable, the amplitudes of these three records were reduced by a constant factor to fit into the pattern.

An obvious feature of the record section is that no recordings were made within 80 km of the shot points. Due to limited time and funds, it was decided to forgo information about the surface layer. Thus, incident energy from the upper crust never appears in the form of first arrivals. Records from 80 - 150 km show a branch of first arrivals with an apparent velocity of 6.5 - 6.6 km/s and an intercept of 1.25 ± 0.15 sec. Although the first arrival at C13 was emergent, it was picked with a high degree of confidence from the analog record. This branch of first arrivals has been interpreted as the head wave (P_g) propagating along the surface of the crystalline basement beneath the Rocky Mountains. It should be noted that the higher frequency energy apparent in A3 and B3 is due to the source effect of the Fording explosion; traces A2 and A3 were recorded at the same location, as were B2 and B3. With one exception, records from 80 - 150 km seemed to show no coherent branches of upper crustal energy. The exception is the strong high frequency phase recorded on A3 at a

Figure 6. Normalized record section with no correction for geometrical spreading.

28

Figure 7. Normalized record section with correction for geometrical spreading.
Amplitudes are multiplied by the square of the distance from shot point.
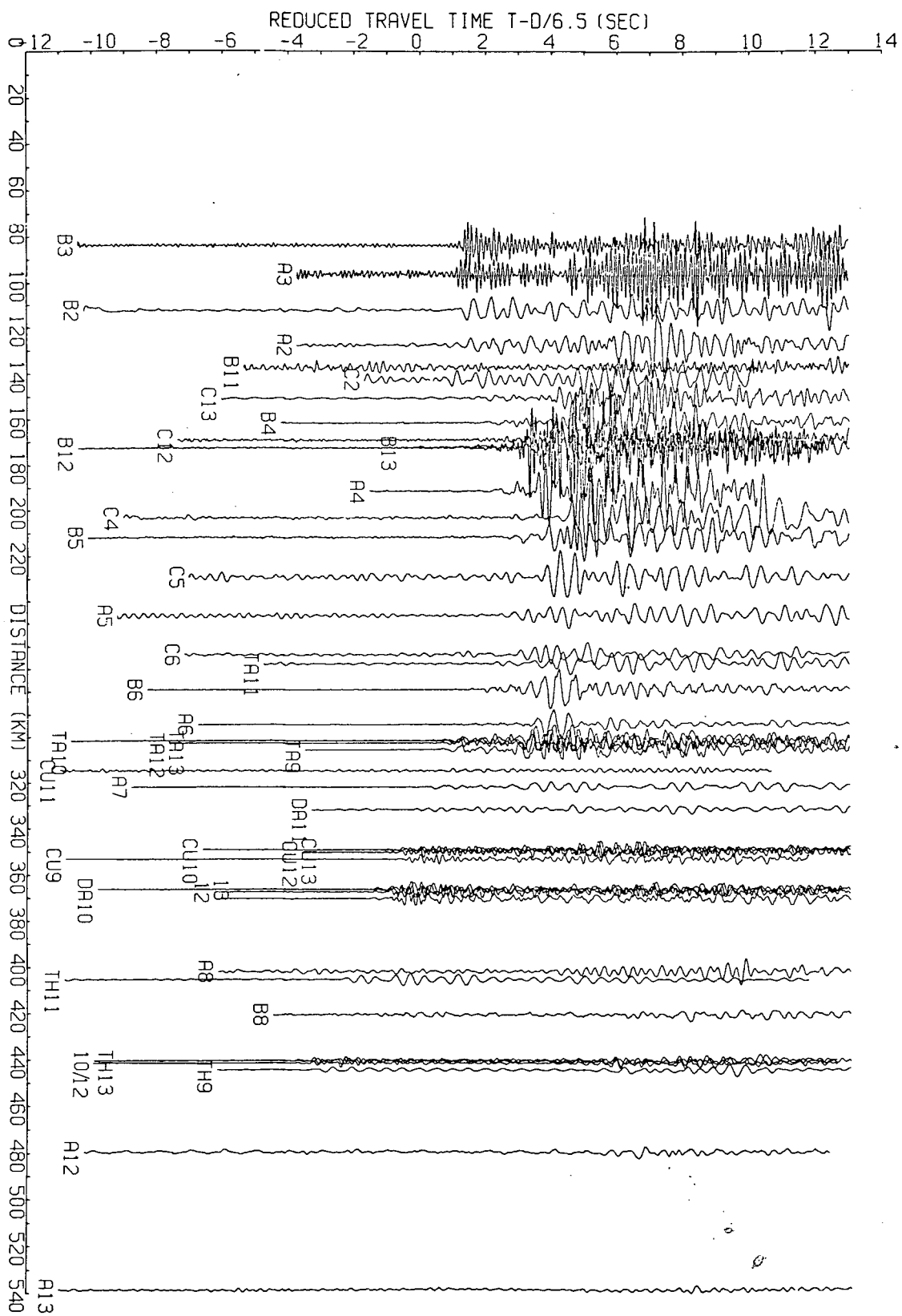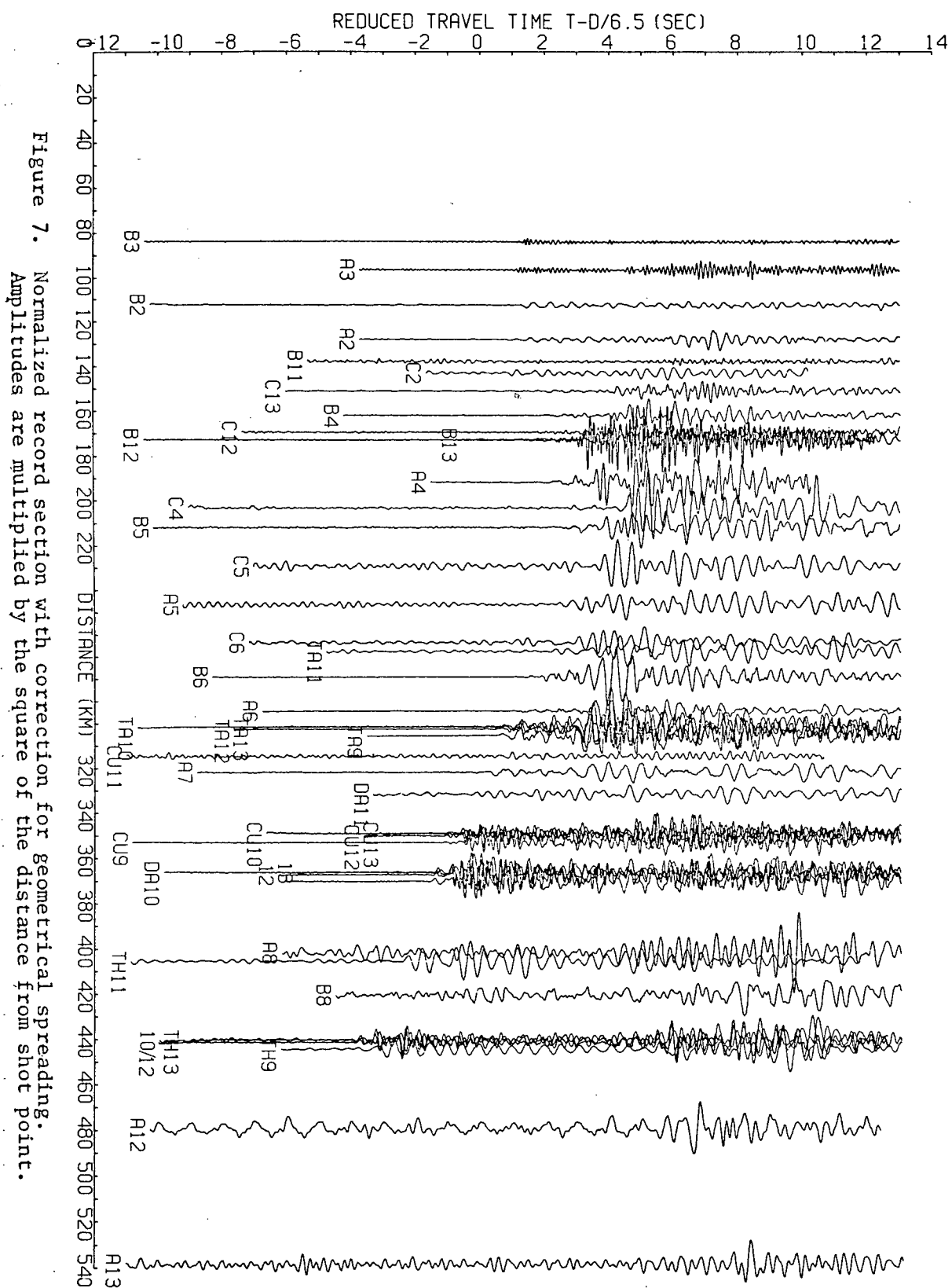
reduced traveltime of 4.5 sec and on A2 at 5.75 sec, giving an apparent velocity of approximately 5.0 km/s. The high frequency character of this phase at A2 has been attenuated by filtering in order to improve the quality of the first arrival. It has been interpreted as either an upper crustal phase or a local reverberation.

Perhaps the most interesting phenomenon of the record section occurs from 150 to 200 km amidst a grouping of large amplitude phases. Beyond C13, first arrivals are extremely weak and are delayed from an extrapolated P_g branch by approximately 0.5 sec near 170 km and 1.0 sec near 190 km. On record B12 at 2.9 sec a very strong higher frequency (8 Hz) phase suddenly appears which is not apparent on B13 at exactly the same distance. This phase dies out rapidly beyond B12 to B5, but seems to lie on a branch with an apparent velocity of 6.5 - 6.6 km/s, values identical with those of the P_g phase.

Another striking feature is the large amplitude secondary arrivals from about 160 km to 320 km near A7. These have been interpreted as reflections from the Moho at and beyond the critical angle. Synthetic seismograms to substantiate this interpretation appear later in this section.

Records from 279 to 444 km show a low amplitude first arrival of frequency 3 - 4 Hz, followed 0.5 seconds later by a stronger phase. The apparent velocity of the first arrival phase is 8.22 ± 0.04 km/s with an intercept of 10.3 ± 0.3 sec, and has been interpreted as the head wave travelling along the Moho discontinuity (P_n). As predicted by the head wave coefficient, its amplitude remains relatively constant along the record section corrected by the distance squared factor (Figure 7). Except for an early onset by 0.2 seconds at CUM, this phase lies on a remarkably straight line and has been picked with a high degree of confidence. It probably becomes a first arrival in the vicinity of C5 (230 - 240 km), but timing noise on C5 and C6 and a passing train on A5 have effectively obliterated the evidence. Near 170 km the P_n branch appears to merge with the reflected branch, but this is rather vague. The larger phase 0.5 seconds later than P_n has been interpreted in terms of a low velocity layer beneath the Moho.

Over the last 100 km of the profile a most interesting late phase appears. It is first seen with confidence at THO, approximately 9 - 10 seconds after P_n. The same phase is prominent on A12 and A13;

all three appear to lie on a line (slightly concave upward) with
apparent velocity 5.6 ± 0.1 km/s and intercept -6.0 ± 1.7 sec.
It intersects the P_n branch at 277 ± 13 km and may be related to the
large amplitude, long duration 4 Hz phase on A8 at a reduced traveltime
of 4 sec. Evidence for an interpretation of this arrival as a converted
phase will follow.

Finally, the last feature of note is the significant change
in noise levels north of DAI. Immediately south of this region, records
B6, A6 and A7 show excellent signal-to-noise ratios, as do the Mica
sites TAB, CUM and DAI. All three field sites were located on the
valley floor and B6 was not even on bedrock. However, A8, B8 (also B7,
not shown), A12 and A13 indicate a much higher background noise level,
even though only A8 was not located on bedrock. Even THO records show
a noisier character than do the other three Mica sites. A very tentative
suggestion is that this increase in noise level may be related to the
occurrence of Proterozoic gneissic rocks which outcrop only in a small
zone around A8, B8 and at THO (Geological Map of Canada). All sites
south of DAI are located on lower Paleozoic sedimentary rocks.
In addition, sites A12 and A13 appear to be located along a long belt of
mainly metamorphosed Hadrynian sedimentary rocks which occur nowhere
else to the south in the Trench. This may be an indication either of
poor coupling to basement rocks or of a shattered character in the
surface rocks.

Interpretation technique

Interpretation of the data in terms of crustal structure
relied heavily upon a computer routine (HRGLTZ) developed by R.A. Wiggins.
A table of p-delta values is initially constructed from the data by
evaluating the slopes of the traveltime branches in the record section.
After this the program produces velocity-depth and T-delta curves based
on Weichert-Herglotz integration and geometric ray theory. Provision
exists in the program for low velocity zones but not for lateral inhomo-
geneities such as faults. The program also calculates synthetic
seismograms based on the quantized ray theory of Wiggins and Madrid (1974),
although this technique is only approximate near large discontinuities
in velocity.

Structure based on arrivals from 0 to 150 km

Since the Trench is a detritus-filled feature and since many sites were not located on bedrock, a sediment thickness of about 200 meters with velocity 3.3 km/s (Lamb and Smith, 1962) was assumed. P-delta values corresponding to this velocity were included in the table and manipulated so that HRGLTZ produced the assumed thickness (Figure 8). However, inclusion of this layer has relatively little effect on the rest of the profile, increasing the intercept times of later branches only slightly.

The first problem encountered was to deduce a reasonable estimate of the upper crustal velocity. As mentioned earlier, records A2 and A3 show significant secondary energy with an apparent velocity of 5.0 km/s. Consequently, a model was attempted with a 5 km/s layer above the 6.5 km/s zone (dotted lines if Figure 8). The upper T-delta plot in Figure 9 shows the best fit of the two branches to the data, using a short period (T = 0.125 sec) Gram-Charlier wavelet with sharp onset to simulate the high frequency energy of the 5 km/s branch and the Fording source energy. As described by Jones and Morrison (1954), a Gram-Charlier wavelet is the negative sum of the fifth and sixth derivatives of the Gaussian error function. Figure 6 should be used for comparison since the HRGLTZ routine does not compensate for geometrical spreading. A relatively sharp gradient was introduced to increase the amplitudes of the reflected branch, in keeping with the large energy on the section. However, even if the 5 km/s branch is extended further, the secondary synthetic amplitudes are not as large as desired. Doubt about the validity of this branch is increased when it is observed that this phase only appears at the one recording location, and may just be a local reverberation. Finally, its associated velocity is lower than has been determined for the upper crust by other workers in the area.

Chandra and Cumming (1972) obtained a velocity of 6.16 km/s in the foothills of central Alberta, while Forsyth (1973) used a value of 5.6 km/s for an area about 200 km west of the Trench an 53°N. However, it was felt that the velocities of 5.2 - 5.5 km/s obtained by Lamb and Smith (1962) in the Trench were more applicable. The higher velocity of 5.5 km/s (p = 0.18 s/km) was then chosen as a compromise and included in the p-delta table (solid line in Figure 8). Some form

33
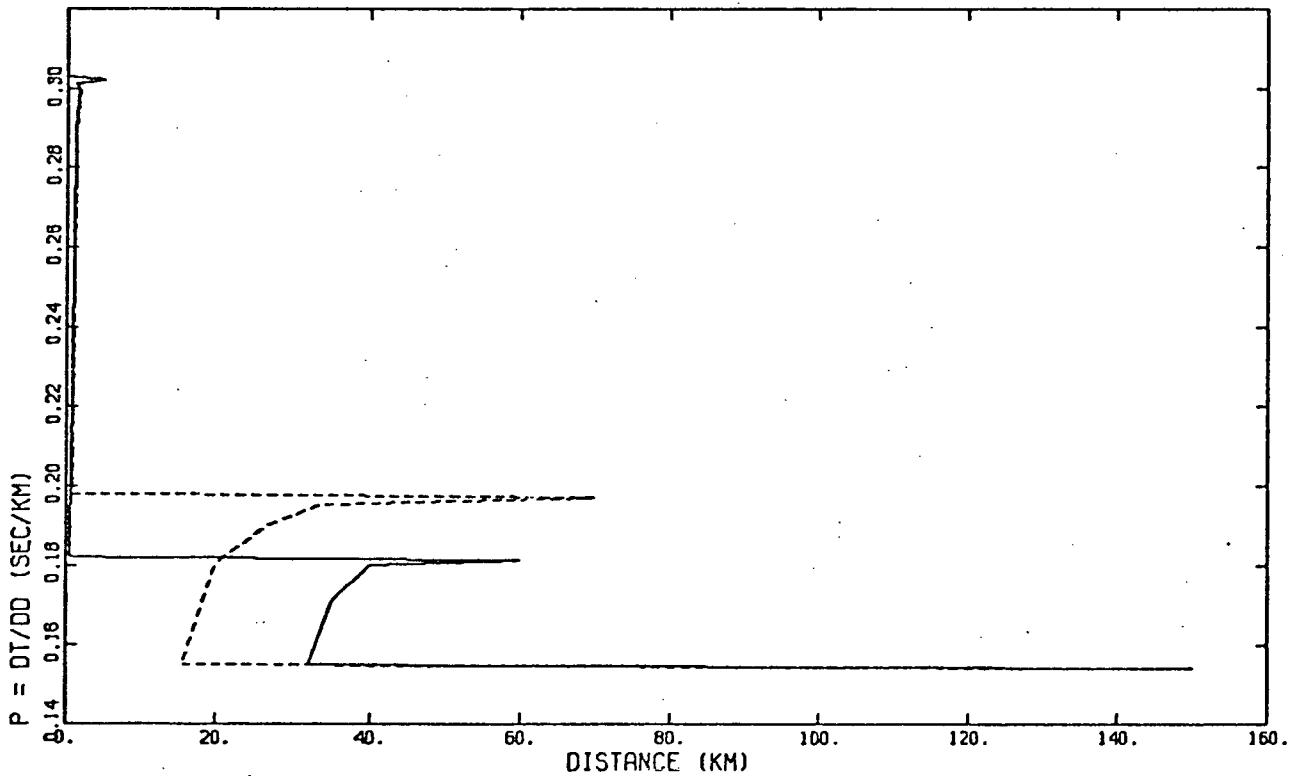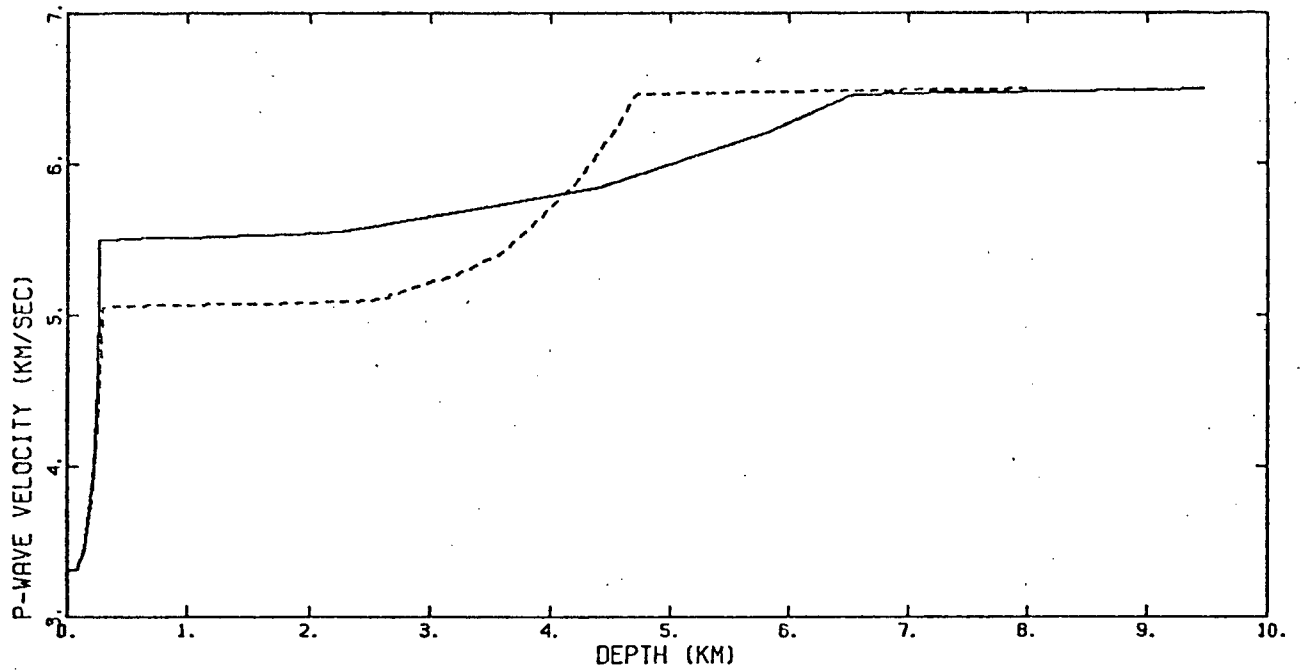
Figure 8. Velocity-depth structure and p-Delta curves
for two basement models.
Dotted line is the 5.0 km/sec model.
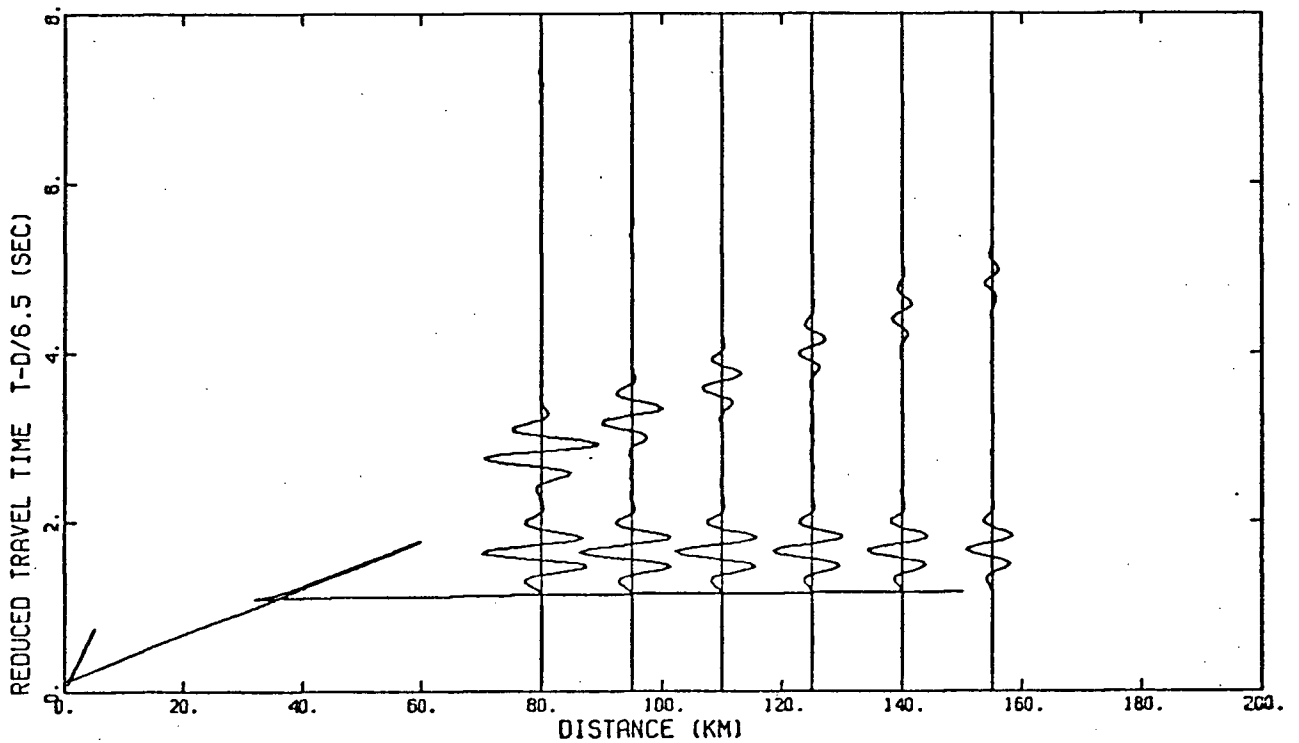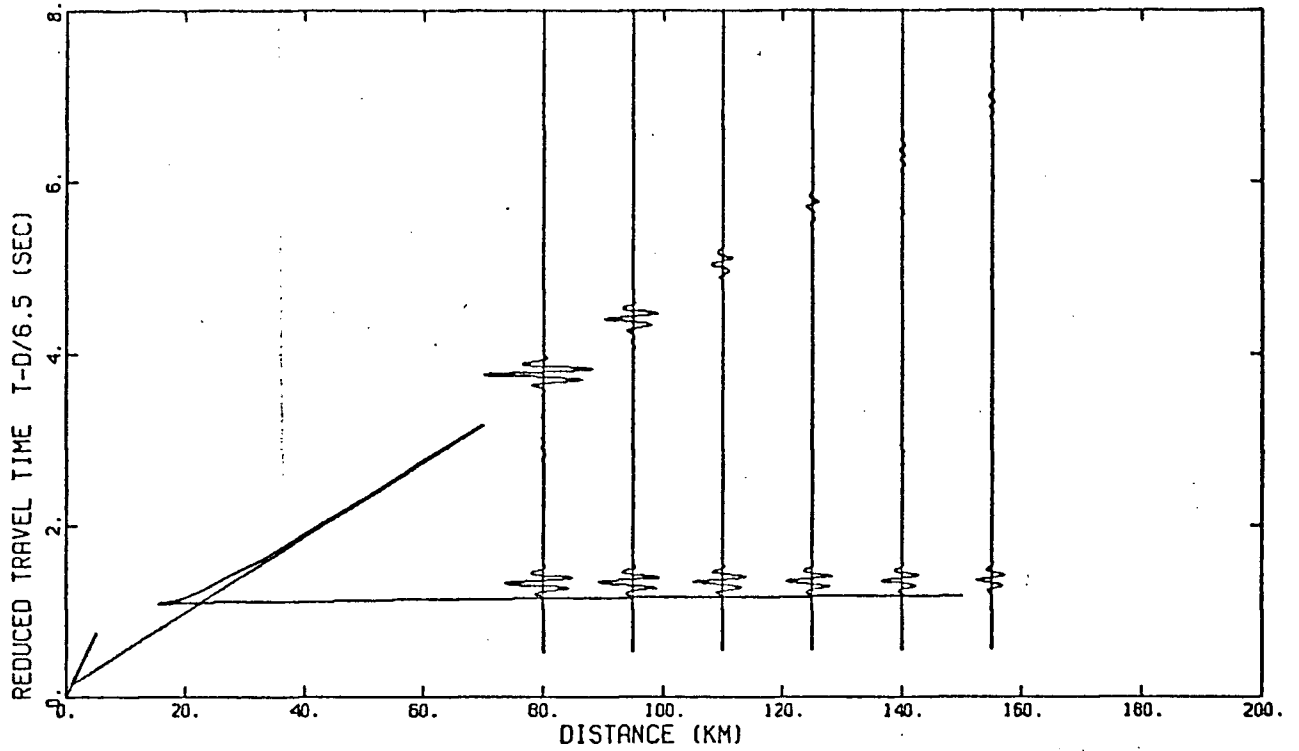Solid line is the preferred 5.5 km/sec model.

Figure 9. Synthetic seismograms for the 5.0 km/sec model (top)
and the 5.5 km/sec model (bottom).
A Gram-Charlier wavelet with sharp onset is used.
The higher frequency wavelet corresponds to energy from
Fording, whereas the lower frequency corresponds to
energy recorded from Kaiser.

of smooth velocity gradient is necessary in order to reduce the secondary amplitudes, since no coherent 5.5 km/s branch is seen in the data. Even so, the synthetic seismograms of the lower plot in Figure 9 show secondary amplitudes slightly larger than desired. This is probably due to the lack of a constant unique velocity in the highly deformed upper crust. (The same form of wavelet as before was used with T = 0.35 sec to simulate the observed frequencies from Kaiser.) Qualitatively then, the velocity-depth structure shown by the solid line in Figure 8 was chosen as the most reasonable fit. This gives an average velocity, including the gradient, of 5.7 km/s to a depth of 6.5 km. Underlying this layer is the basement with velocity 6.5 km/s. As can be seen from Figure 1, this is the basement depth beneath the Western Ranges of the Rockies in this region, and not the depth to basement beneath the Trench.

Low velocity zones

The next problem was a suitable explanation for the time delay beyond 150 km. This phenomenon can be interpreted as the "shadow zone" effect of a low velocity layer, and a model with this structure has been achieved. Credibility is lent to this hypothesis by recent interpretations in a similar vein (e.g. Berry and Fuchs, 1973). A low velocity zone beneath the Moho will be described after the upper crustal zone.

A time increment of 1.75 sec was chosen from the record section for the "shadow zone", this being the time delay between the traveltime branches at 150 km and 230 km (Figures 10, 11a). This produced an extremely thick (15.5 km) layer of velocity 6.1 km/s at a depth of 9.1 km (Figure 10). To simulate the curvature and large amplitudes of the reflected branch from the Moho, a linear decrease in p was modelled (from 300 km to 170 km in Figure 10), producing a velocity gradient from the low velocity zone at a 24.6 km depth to the Moho at 56.2 km.

A fit of the traveltimes to the record section is quite good (Figure 11a). Since the HRGLTZ routine does not compensate for geometrical spreading, the corresponding uncorrected record section was used for comparison with the synthetic plot (Figure 11b). On the record section note especially how at distance 300 km the later "P_g" branch merges smoothly into the wide-angle reflections from the Moho,
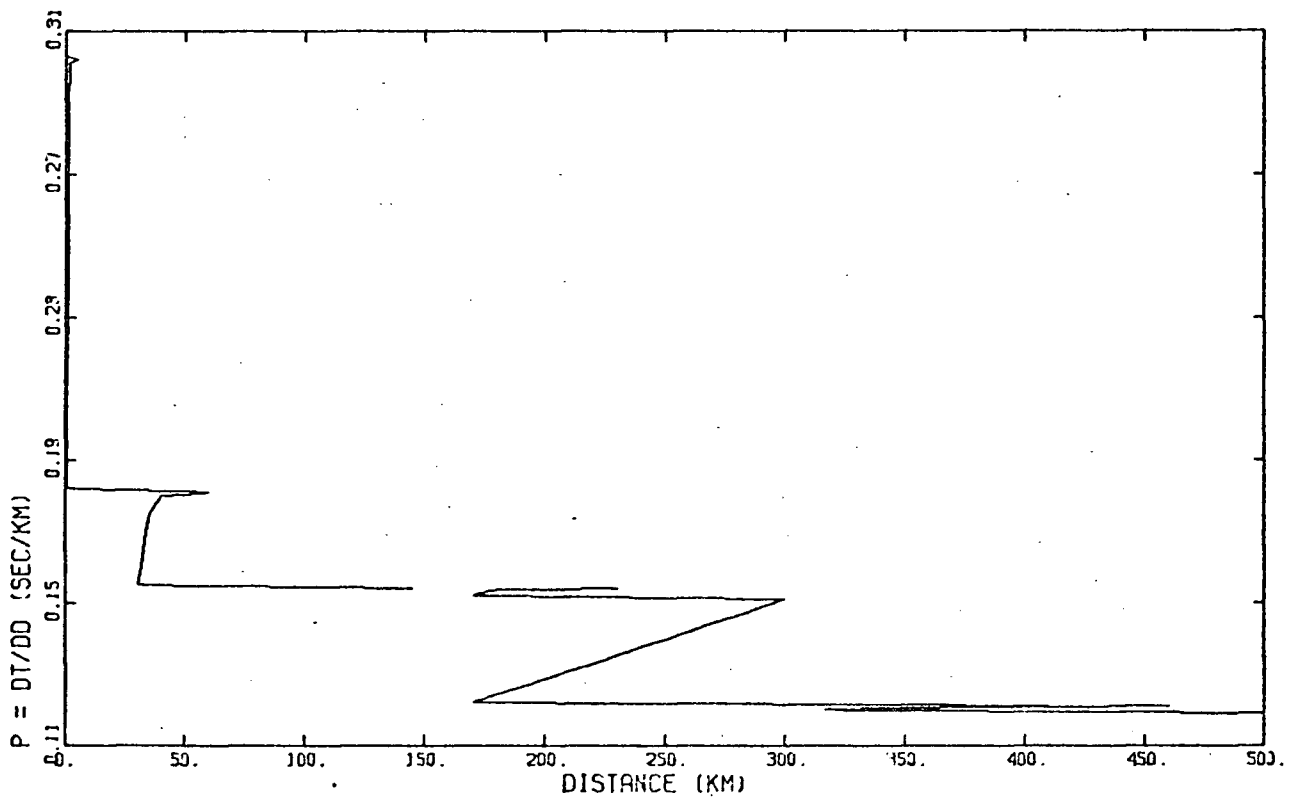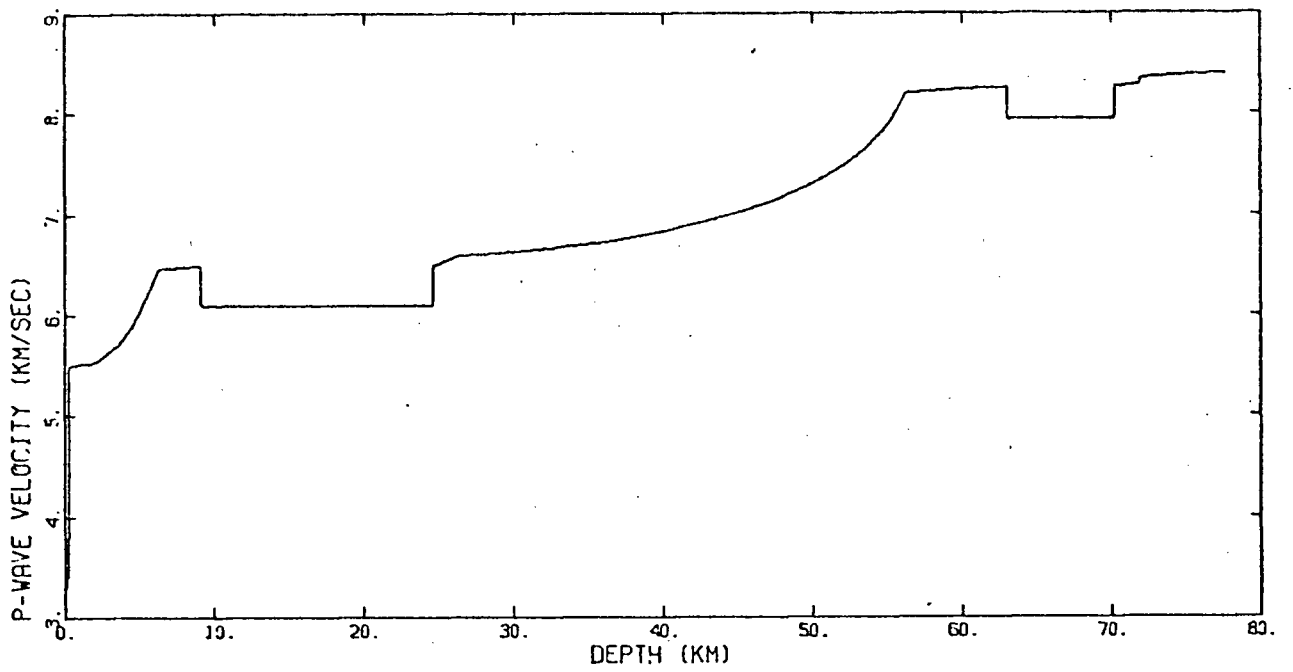
Figure 10.   Velocity-depth structure and p-Delta curve
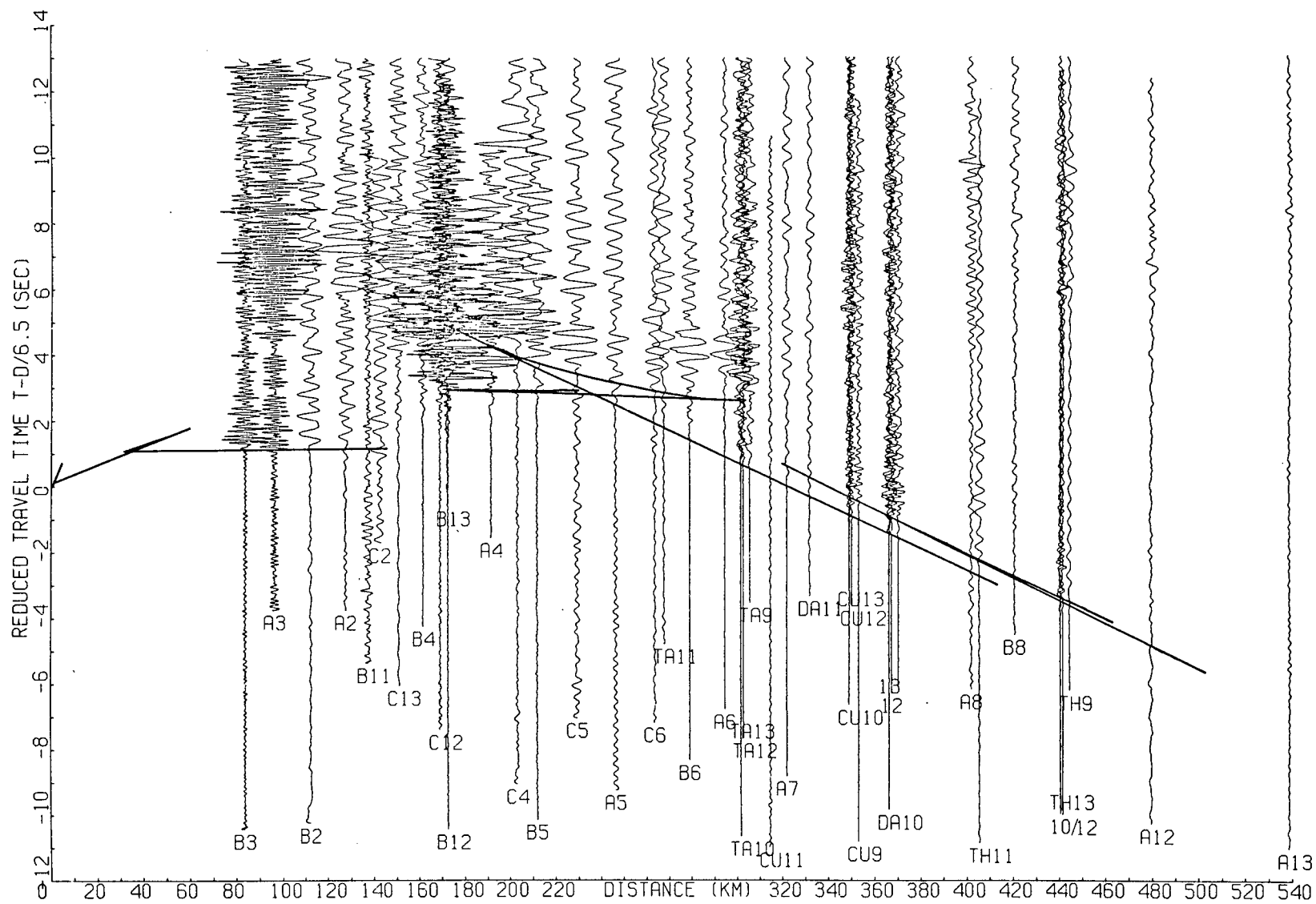for the low velocity zone interpretation.

Figure 11a.   Fit of travel-times to the record section for the low velocity zone interpretation.
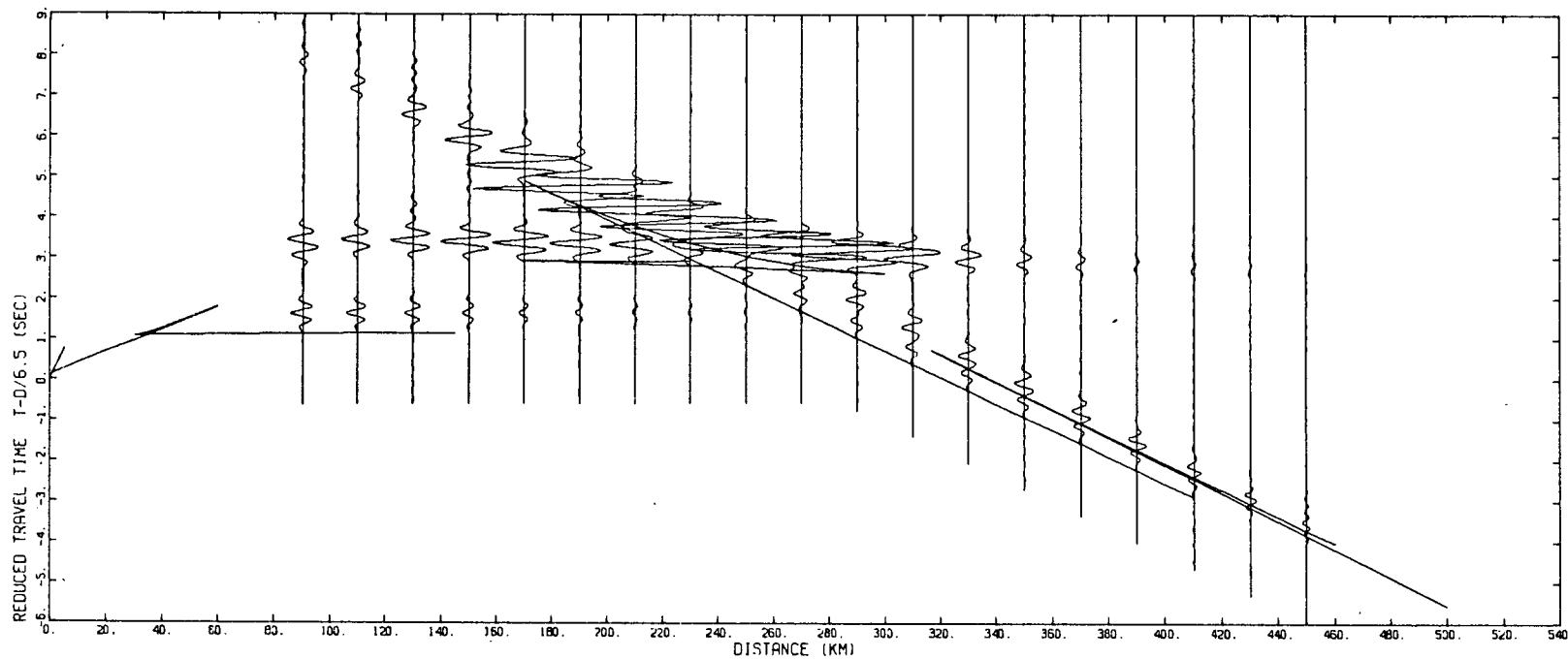
Figure 11b. Synthetic seismograms for the low velocity zone interpretation.
A "Kaiser" Gram-Charlier wavelet is used.

38

adding confidence to the interpretation of this "P_g" branch. Also note that the largest reflected amplitudes (on A4 and C4) occur approximately 30 to 40 km beyond the critical point. This result agrees with the work of Cerveny (1966) who showed that, for a 3 - 4 Hz frequency and a refractive index of 0.80 - 0.83 at the Moho, the maximum amplitude should appear about 40 km beyond the critical point.

With two notable exceptions, the synthetic seismogram section of Figure 11b shows good agreement with the data. On the positive side, the traveltime curvature and amplitudes of the Moho reflections agree well, as do the amplitudes of the P_n arrivals. However, the first exception to the fit is that the amplitudes of the P_g branch between 30 and 140 km do not attenuate as rapidly beyond 140 km as is indicated by the data. As expected, it also does not fit the observed time delay of the faint first arrivals behind an extrapolated P_g branch in this region. This may be due to the inherent inaccuracy of the HRGLTZ routine or it may be evidence for lateral inhomogeneities. A similar conclusion can be reached for the second exception: although the later "P_g" branch on the synthetic record section does show a large amplitude at 170 km, the amplitudes at some distance to either side are also quite large. Although the data show a large amplitude near 170 km (B12), there is no evidence for energy corresponding to this phase arriving before 170 km, and "P_g" amplitudes beyond 170 km are strongly attenuated.

Noting the fact that no other studies have found such a thick low velocity zone in the upper crust, the fact that it may be petrologically impossible, and the imperfect fit of the synthetic seismograms, the interpretation of a sub-basement low velocity zone was rejected in favour of a model involving lateral structural changes.

However, the interpretation of a sub-Moho low velocity zone seems more plausible. After a suggestion derived from Barr (1971), the strong energy 0.5 seconds after P_n was modelled as an effect of a low velocity zone immediately underlying the Moho. This essentially means that body waves refracted just beneath the Moho are delayed slightly by the low velocity zone, and exhibit practically the same apparent velocity as the P_n phase. A layer 7.2 km thick, with velocity 7.9 km/s, at a depth of 63.0 km gives the best fit. The synthetic record section in Figure 11b shows that this secondary phase is parallel to the P_n branch and has significantly larger amplitudes beyond 280 km - features which are evident in the record section of Figure 11a.

Fault models

A downthrown fault will introduce a discontinuous delay in the traveltime curve. A technique developed by the writer, details of which are given in the Appendix, enabled the use of the HRGLTZ routine to model this type of discontinuity.

The purpose of the technique is to produce a down-fault velocity-depth structure. However, the HRGLTZ routine calculates horizontally layered models only, so that there must be a time difference between the actual traveltime branches in the data and the traveltime branches calculated by HRGLTZ for a down-fault structure. Making certain assumptions about the ray paths beyond a fault, this time difference can be calculated. The HRGLTZ routine then gives the down-fault depth, from which the throw of the fault can be calculated. However, a word of caution is advisable since several assumptions are made. One is that the shot point-to-fault distance must be much greater than the fault throw. As borne out by the results, this assumption is valid. Secondly, average velocities for the two crustal layers are used, introducing a certain amount of inaccuracy in calculating critical angles. Thirdly, the basic traveltime equations of geometric ray theory are used, even though a detailed understanding of ray behaviour at a lateral discontinuity has not been developed adequately. Since the HRGLTZ routine does not handle lateral inhomogeneities, synthetic seismograms are not relevant. Only the traveltimes and a qualitative discussion of amplitudes are meaningful.

Such a discussion of amplitudes is perhaps appropriate before a description of the traveltime plots. From 150 km to 220 km the first arrivals are very weak and appear to drift upwards until they are no longer apparent past A4 (Figure 7). This weak phase could be interpreted as a diffraction from the upper edge of the fault. The strong anomalous amplitude on B12 can tentatively be explained as a focussing effect of rays incident upon the concave lower edge of the fault (Barr, 1971). This phenomenon would tend to be very localized and would not appear on adjacent records. There is no such large amplitude at B13, although the distance from the shot point is the same as B12. This could indicate a difference in shape of the fault surface beneath these sites, since they were located several kilometers apart within the Trench.

Three crustal models will be described. The first assumes
a basement fault which does not extend to the Moho; the second assumes
a uniform fault throughout the crustal section. The third model
calculates the fault throw at the Moho based on an assumed up-fault
reflection from the Moho.

Section 1 of the Appendix outlines the method by which the
fault throw on the basement was calculated. Assuming that the 6.5 km/s
branch beyond 170 km has been delayed by the fault, then a HRGLTZ
branch which is 0.89 sec sooner will give the down-fault structure.
The down-fault depth to basement is 12.1 km, giving a fault throw of
5.6 km.

Section 2.1 explains the necessary corrections which must be
applied to the P_n intercept if it is assumed that the fault does not
extend to the Moho. Using a similar argument to the above, the P_n
intercept of the HRGLTZ model must be delayed from the P_n intercept
in the data by 0.54 sec. The dotted line in Figure 12a represents
the up-fault structure, showing that the 6.5 km/s layer extends with
a velocity gradient from 6.5 km depth to 61.2 km at the Moho.
The down-fault structure (solid line in all diagrams) has a similar
crustal thickness, and shows the fault throw of 5.6 km at the basement.
As explained earlier , the velocity gradient is necessary for a correct
fit of amplitudes and curvature of the Moho reflections. Figure 12b
shows the corresponding traveltimes superimposed, for clarity, upon
the record section corrected for geometrical apreading. Except for the
up-fault P_g intercept, all other model branches are parallel and
delayed from the data traveltimes by the amounts calculated.

Section 2.2 of the Appendix details the calculations made
assuming the fault, as calculated previously, extends throughout the
crustal section with a constant throw of 5.6 km. For this case, the
P_n branch in the data is delayed by 0.01 sec from the HRGLTZ P_n branch.
Figures 13a and 13b show the up-fault and down-fault structures and
the traveltimes which result. Up-fault the 6.5 km/s layer extends from
a depth of 6.5 km to 52.2 km at the Moho. The corresponding layer in
the down-fault structure extends from 12.1 km to 57.8 km. Again,
a gradient must be included above the Moho.

The third model was an improvement on the second in that it
was an attempt to determine independently the throw of an assumed fault
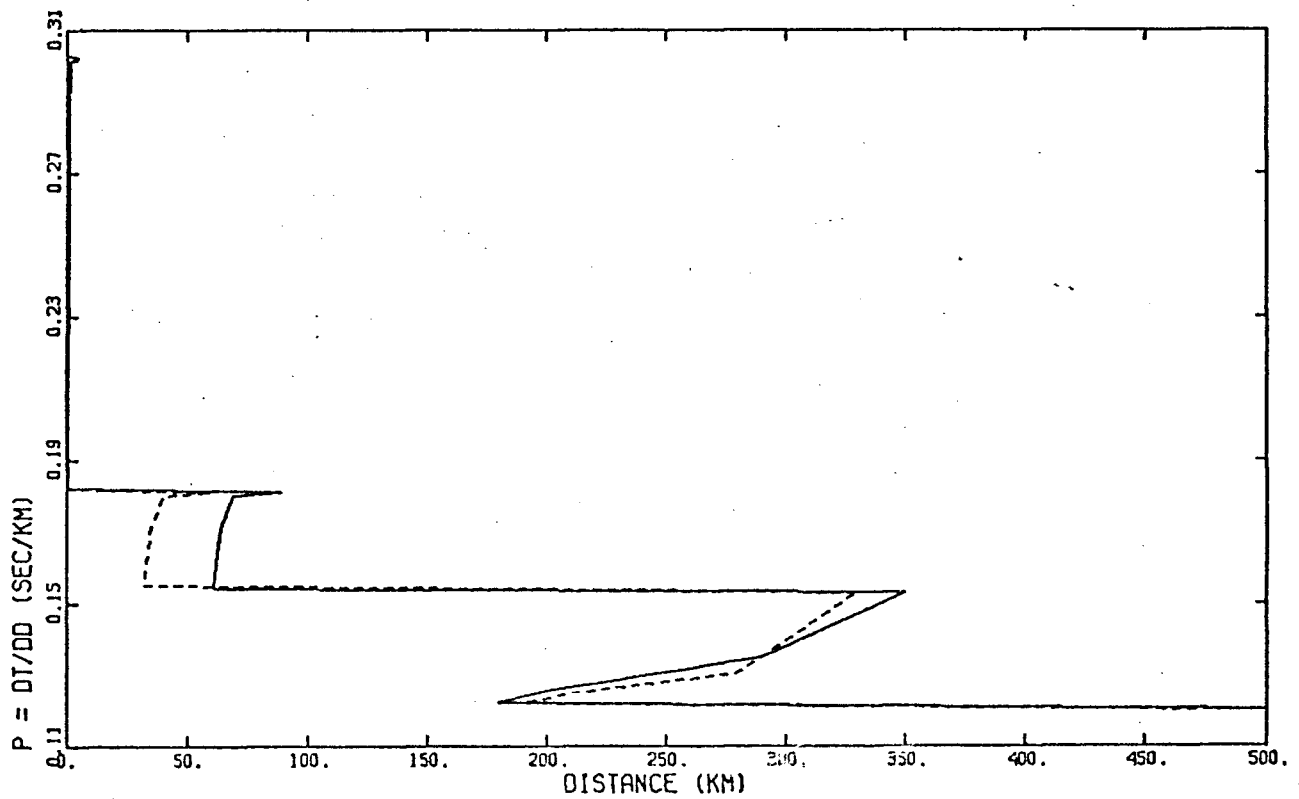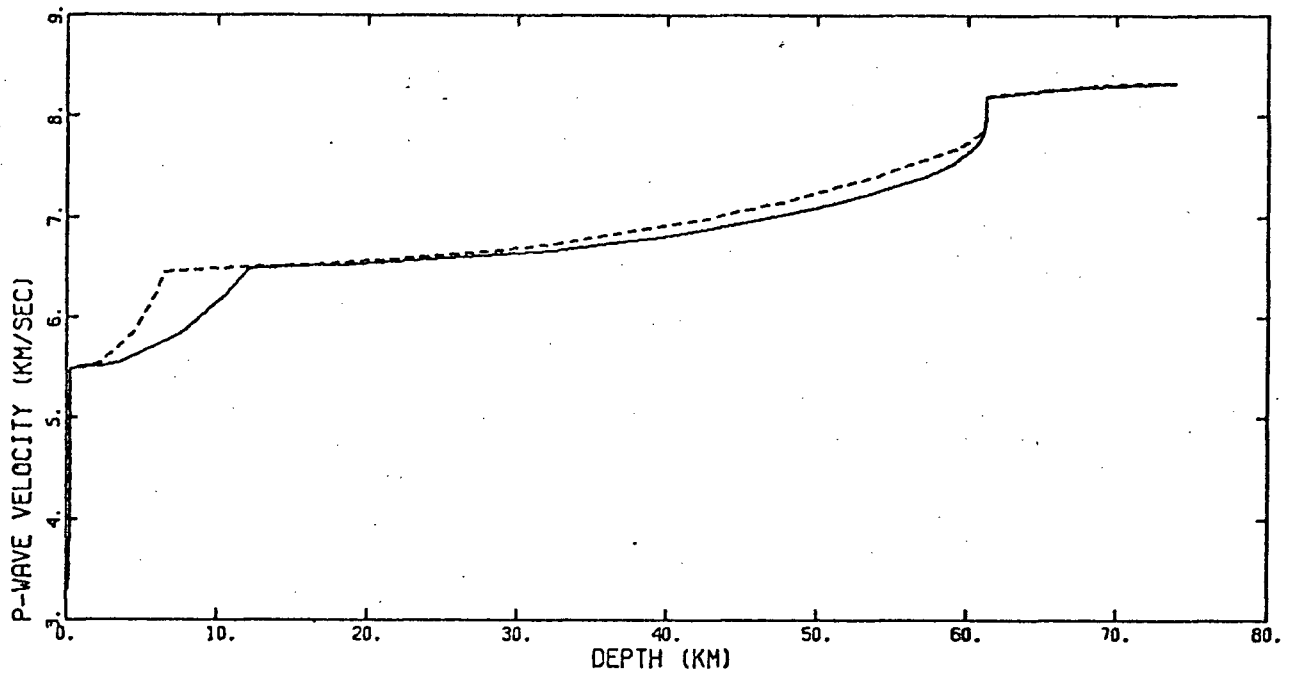
Figure 12a.   Velocity-depth structure and p-Delta curves
              for a model with a basement fault and an
              unfaulted Moho.
              Dotted lines represent the up-fault model.
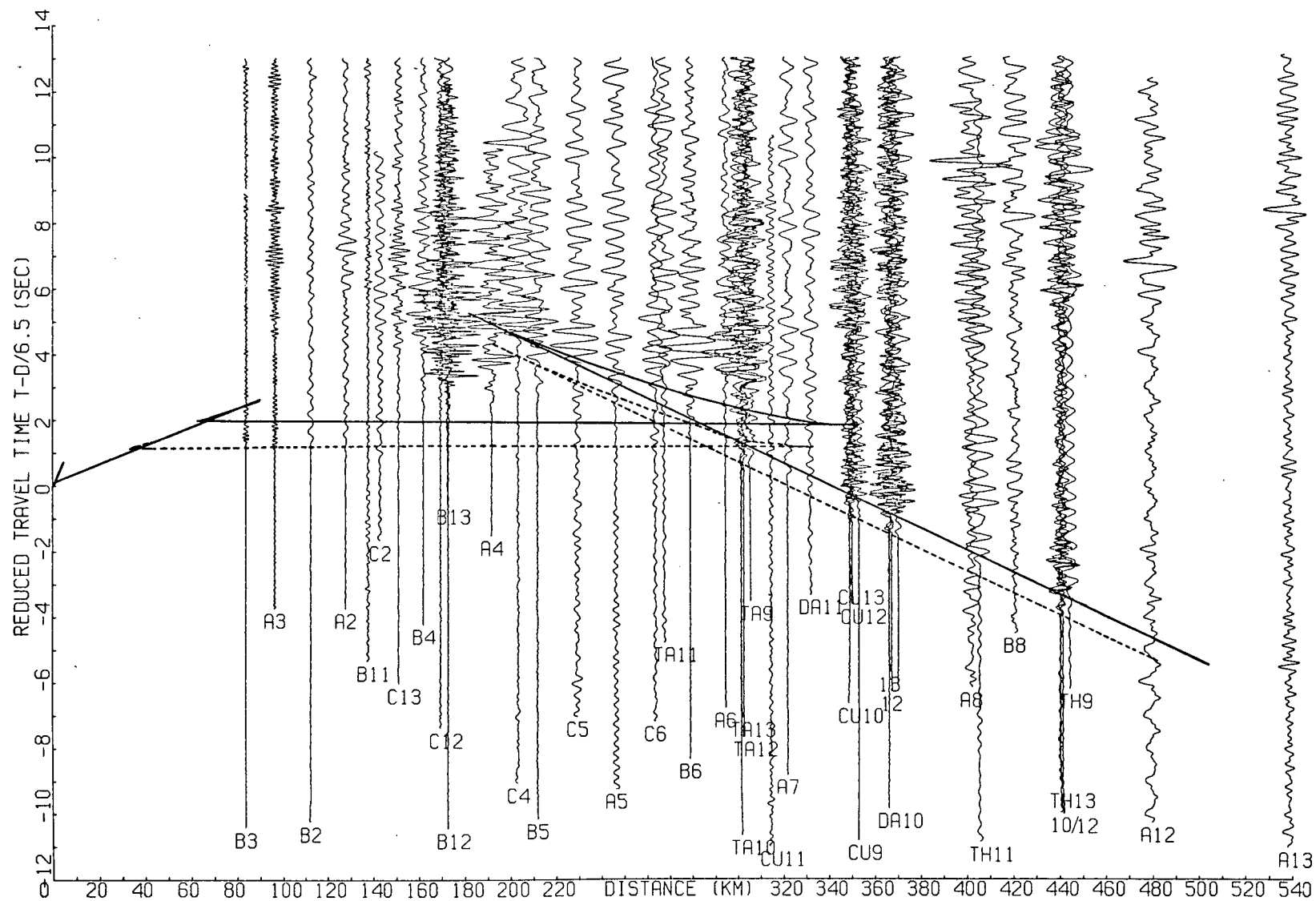
Figure 12b. Traveltime curves for the velocity-depth structure in Figure 12a. Dotted and solid lines indicate traveltimes for models based on the up-fault and down-fault structures, respectively. Model traveltimes are offset from the actual data to account for the perturbed ray paths due to the fault. These models assume that the basement fault does not extend to the Moho.

43
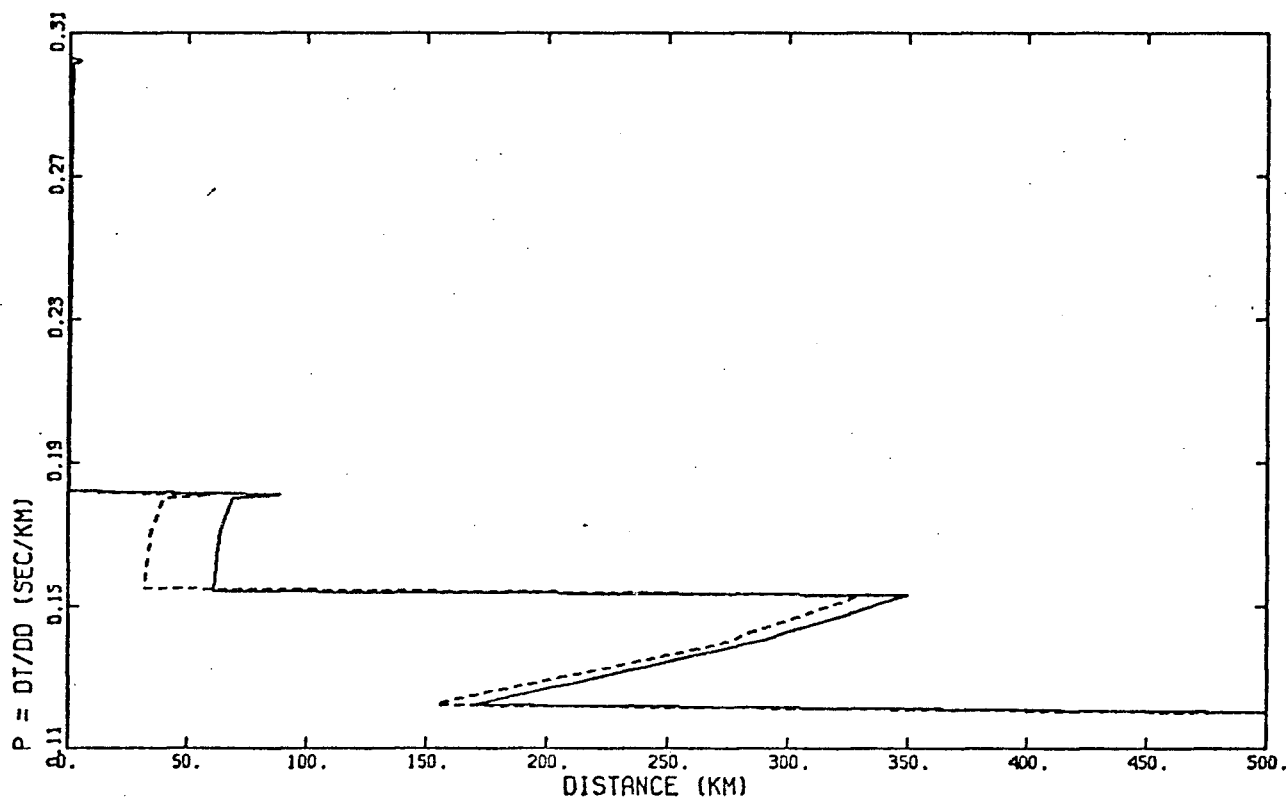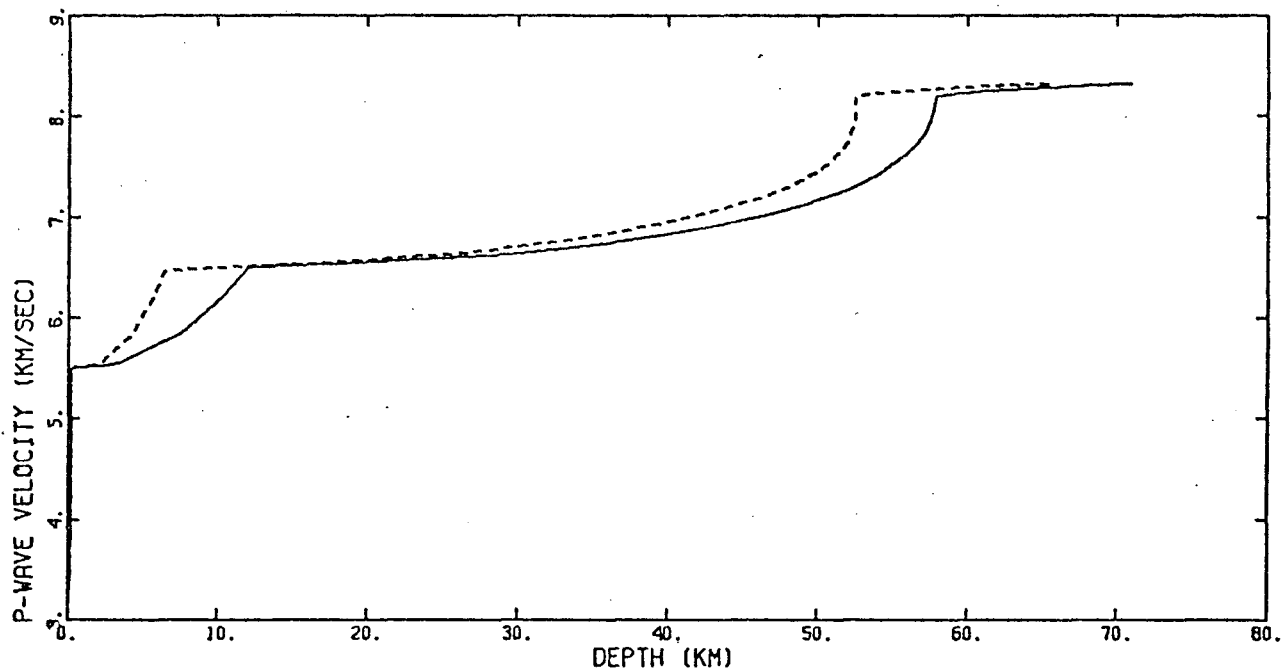
Figure 13a.   Velocity-depth structure and p-Delta curves
for a model with constant fault throw throughout
the crustal section.
Dotted lines represent the up-fault model.
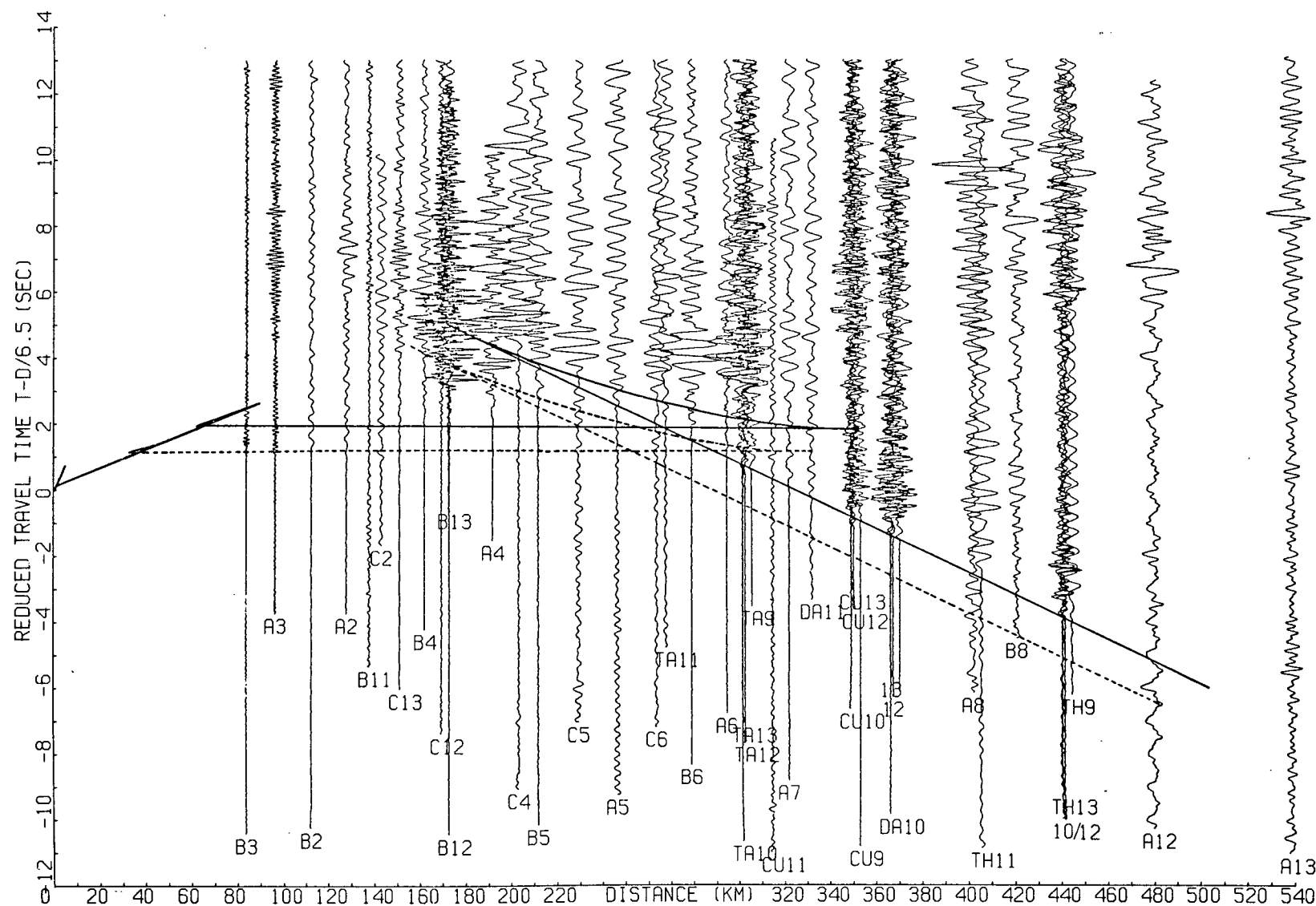
Figure 13b. Traveltime curves for the velocity-depth structure in Figure 13a. These models assume a fault of constant throw throughout the crustal section.
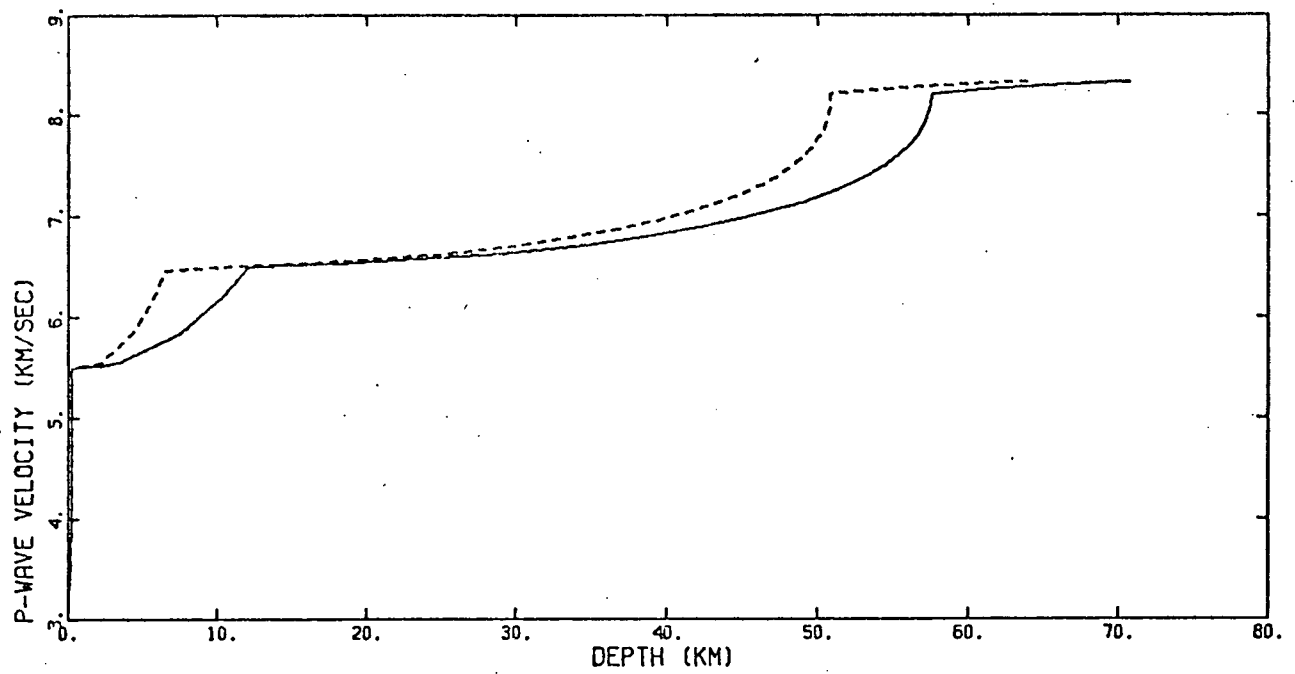
Figure 14a.   Velocity-depth structure and p-Delta curves
for a model which fits an assumed up-fault
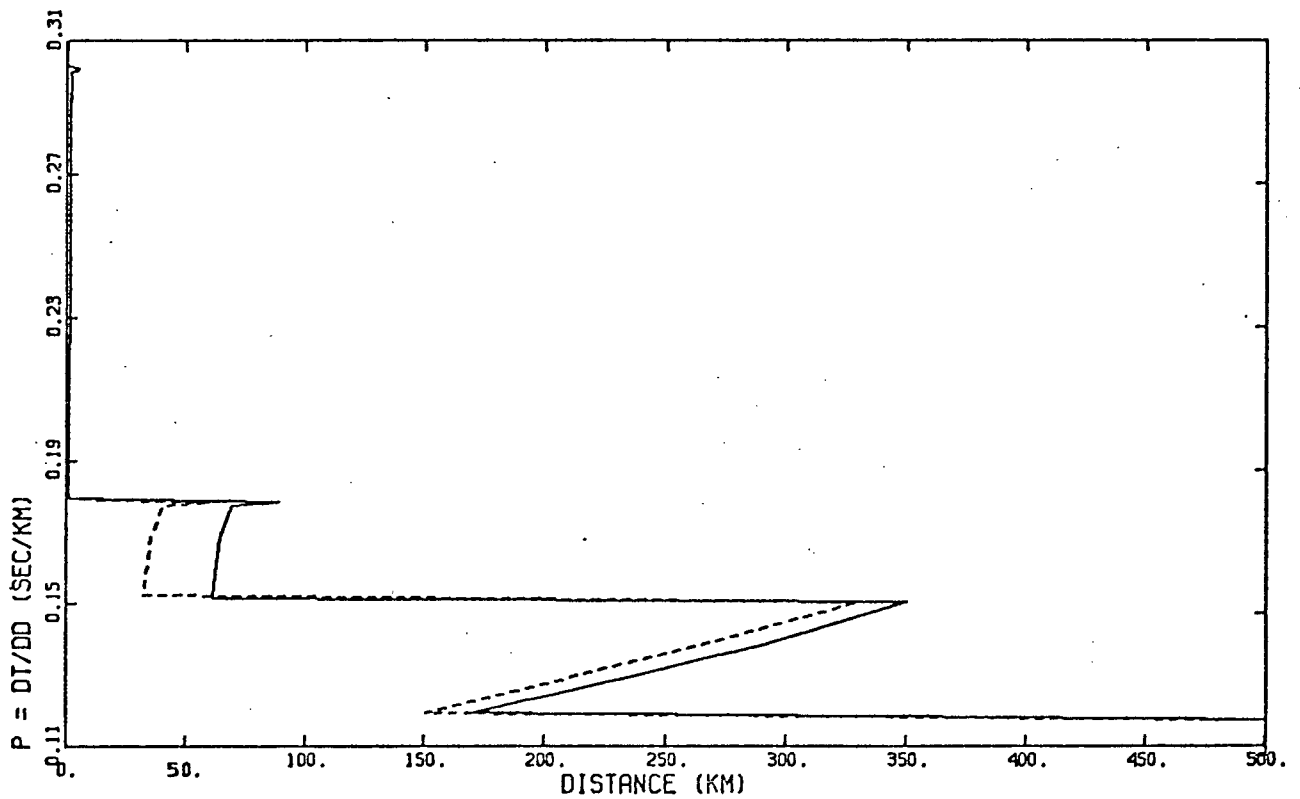P_n intercept.

Dotted lines represent the up-fault model.
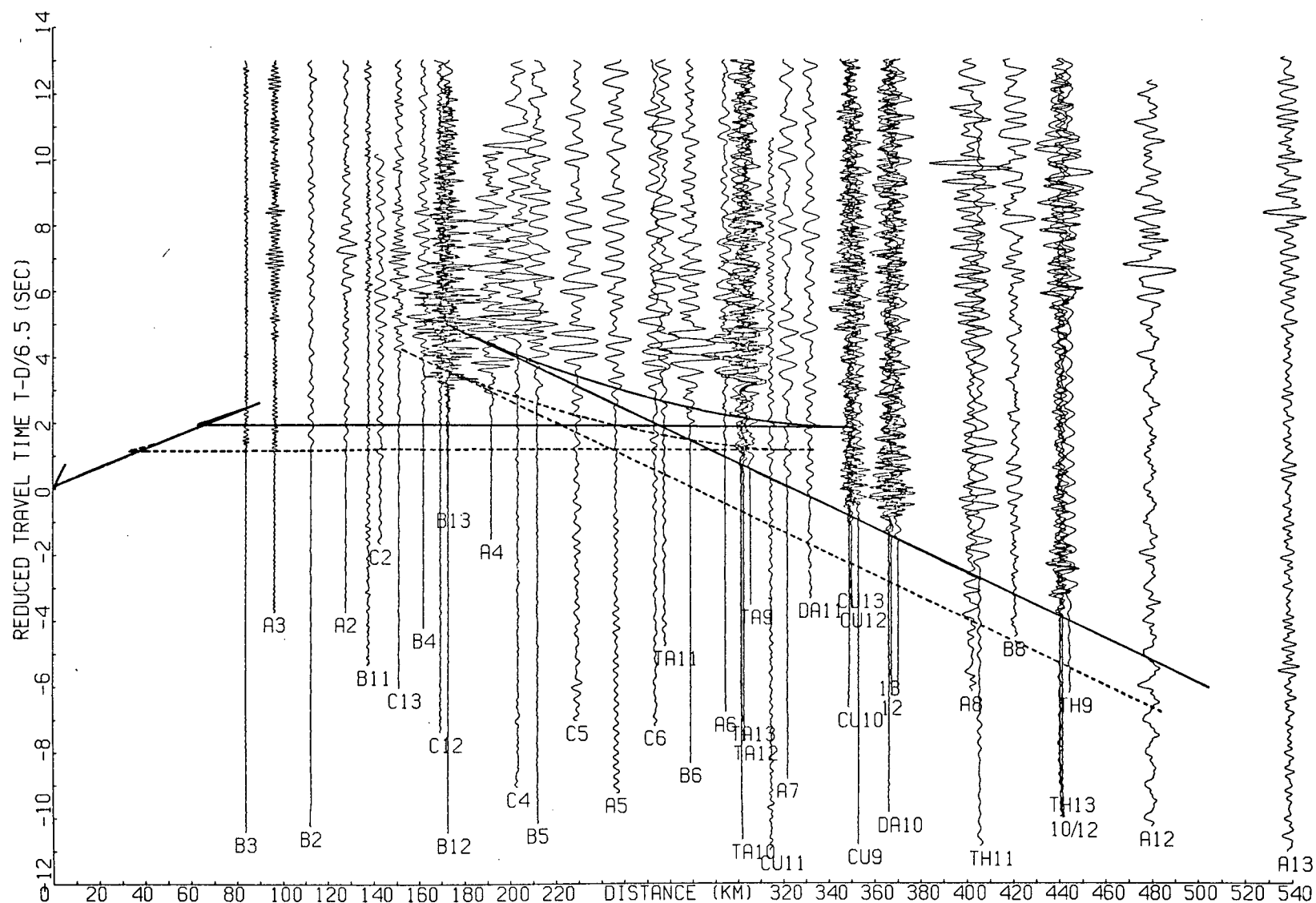
Figure 14b. Traveltime curves for the velocity-depth structure in Figure 14a. These models assume that the secondary arrival on C13 and B4 is an up-fault reflection from the Moho.

on the Moho. It was based on the assumption that the secondary energy of C13 and B4 represented near-critical angle reflections from the up-fault Moho. From the previous two models the critical point can be expected in the range 147 - 174 km; C13 and B4 are located at 151 km and 162 km, respectively. The amplitudes are not overly large in relation to the down-fault reflected branch, as expected for records at the critical point (Cerveny, 1966). The delay time between this early "branch" and the later P_n branch was picked from the record section as 1.5 sec. Following the method of Section 2.3, the down-fault Pn branch in the data was delayed by 0.04 sec from the HRGLTZ P_n branch. This gave a down-fault crustal thickness of 57.6 km (Figures 14a and 14b). A HRGLTZ model was then run for the up-fault structure, with a minor delay from the up-fault P_n "branch" to account for the different thickness of the down-fault upper crustal layer. This gave an up-fault crustal thickness of 50.8 km, and a resulting fault throw on the Moho of 6.8 km.

Late arrivals beyond 400 km

A further challenge of the section was to interpret the strong phases appearing at reduced traveltimes of 4 to 8 sec on A8, THO, A12 and A13. To this end, particle motion diagrams were made from the analog records. The phase on A12 and A13 showed marked shear wave motion in the vertical-radial plane (Figure 15), but the A8 phase had a rather confused motion. It is most likely a P-wave, although the large amplitude occurring about six seconds after phase onset exhibits S-wave characteristics. The relation between this phase and the S-waves on A12 and A13 has not been resolved. However, lacking any horizontal information from seismograms recorded from THO, these later phases were assumed to be S on the basis of their similar character to the A12/A13 arrivals.

Therefore, it was assumed that this phase had undergone some form of conversion from P to S within or at the base of the crust. Although the idea of a converted multiple has been proposed, only an interpretation as an S_n phase has been attempted. Unfortunately, the P_n phase cannot be picked with any confidence beyond THO, so that the following conclusions are mainly conjectural. However, the weakness of the P_n phase is not surprising, especially if most of the compressional
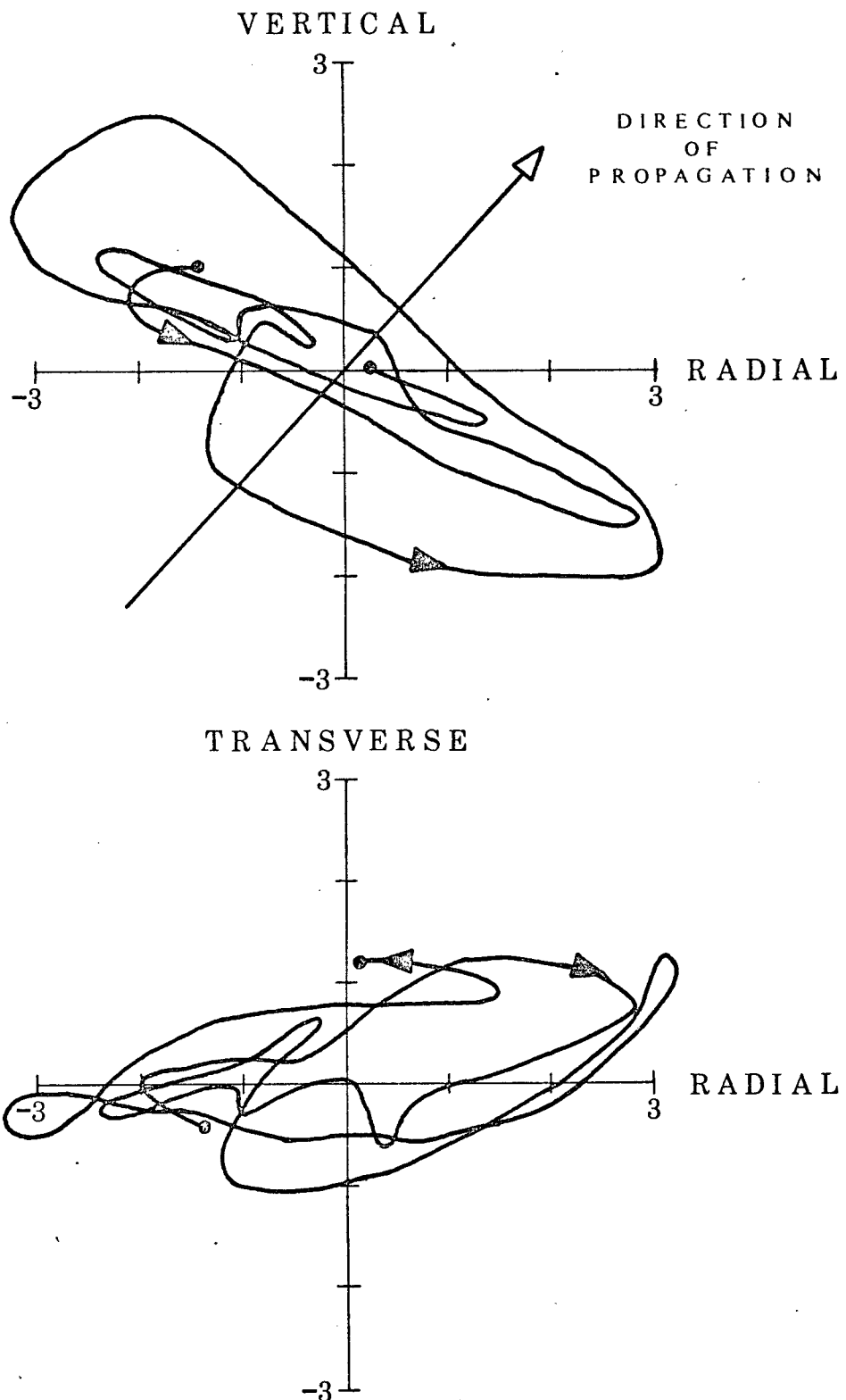
Figure 15. Particle motion diagram of the A12 large amplitude phase
arriving at a reduced time of 7 seconds.

Time span = 1.3 seconds.
1 axis division = 38 millimicrons of ground displacement.

energy has been converted to shear energy.

If it is assumed that this S_n phase first appears at THO, then its delay time from the P_n phase at this point should give an approximation to the depth of conversion. Assuming the crustal velocities of the fault models and a Poisson's ratio of 0.25, a calculation gives approximately 52 km for this depth. This is 6 km less than the crustal thicknesses for models with a faulted Moho. However, it is of the same order of magnitude as the Moho depth calculated for the southern part of the profile. Allowing for the angle of incidence, this conversion would take place in the vicinity of the Moho beneath DAI.

The rather high apparent velocity of 5.6 km/s can be explained by a southeasterly dip on the Moho beyond DAI. Again using average crustal velocities and a Poisson's ratio of 0.25, the required dip would be 11°. Considering the assumptions made, this dip calculation can only be approximate. In addition, it cannot be substantiated by the present seismic data.

DISCUSSION OF THE RESULTS

The basement near $50°30'N$, $115°W$

From the Rocky Mountain Trench seismic data, a depth of
6.5 km to a layer with P-wave velocity 6.5 km/s has been calculated
along a northwesterly-striking line beneath the Western Ranges of the
Rockies. From seismic reflection studies, Bally et al (1966) have
shown that the basement under the western Rocky Mountains near $49°15'N$
dips gently to the southwest. And from a geologic reconstruction,
Price and Mountjoy (1970) reached reached a similar conclusion for the
basement near $51°30'N$. However, since the refraction profile is on
strike with the regional trend of the Cordillera, significant dip along
this line is not expected, and therefore, the apparent velocity of
6.5 km/s is probably close to the true velocity. Data from both
shot points seem to agree, so that these results may be taken as
average values for the region.

As expected for a feature related to the Precambrian Shield,
the basement refractor velocity of 6.5 km/s agrees better with data to
the east than to the west. Chandra and Cumming (1972) have mapped
a 6.5 km/s surface near $50°30'N$ in Alberta, whereas at equivalent
depths in the Intermontane Belt, White et al (1968) and Forsyth (1973)
found velocities of only 6.1 and 6.2 km/s, respectively. A survey
by Hales and Nation (1973) just south and west of the Trench found a
velocity of 6.41 km/s at 22 km depth beneath a 6.0 km/s layer.

The seismic reflection results of Bally et al (1966) indicate
a basement depth in their southern profile of about 7.9 km (26,000 ft)
below a datum at 2000 feet above sea level. According to Kanasewich et
al (1969) and Dragert (1973), a major Precambrian rift zone in the
basement strikes northeast between this region and the area of our
profile. Therefore, it is not surprising that the agreement between
the depth of Bally et al (1966) and that calculated in this study is
not more exact.

It must also be remembered that the depth of 6.5 km is
dependent upon the choice of an upper crustal velocity. Including a
velocity gradient, the average velocity is 5.7 km/s. If this velocity
is too high, then the basement depth may be overestimated by as much
as one kilometer. Unfortunately, the secondary arrival data show no

clear evidence for a uniform velocity with a coherent branch. In such
a complexly thrusted region, this is not unexpected.

Low velocity zones

The upper crustal structure determined with a low velocity
zone is not strongly supported by the writer, since the synthetic
amplitudes fit is not good and the required layer thickness seems
unreasonably large from a petrological viewpoint. However, several
relevant points do merit discussion. Mueller and Landisman (1966)
synthesized evidence for a low velocity zone in the upper crust.
Quoting results form previous workers, they concluded that seismic
velocities in granites go through a maximum at depths of around
5 - 10 km below the surface. Thus, a low velocity zone beginning
at 9.1 km is not unreasonable. In an extensive interpretation of
seismic data around the Grenville Front, Berry and Fuchs (1973) have
included a low velocity channel at a depth ranging from 5 - 12 km
with a maximum thickness of 3 - 5 km beneath the Front itself.
Their conclusion is that this thickening may be an indication that
the Front is a zone of weakness. If this is so, then perhaps a similar
thickening under the Trench is also an indication of weakness.
Citing evidence for the effect of pore pressure on P-wave velocities,
they also conclude that water hydration in the upper crust could
produce a low velocity zone. This situation would arise if the pore
pressure were to increase suddenly in relation to the confining pressure.

Although the sub-basement low velocity zone appears implausible,
the 7.9 k/s layer beneath the Moho fits the data well. Qualitatively,
its thickness of about 7 km is in better agreement with findings that
such petrological changes take place over small distances. However,
a petrologic explanation of this low velocity zone will not be attempted.
Other workers (e.g. Forsyth, 1973) have satisfactorily modelled this
phenomenon by including a velocity gradient at depth beneath the Moho.
However, the resulting triplication does not properly describe the
seeming parallelism of the two branches in the Trench data. It is
also interesting to note that exactly the same arrival pattern was
discovered by Cumming and Kanasewich (1966) and was interpreted as a
conversion at shallow depth in the Cretaceous section of Alberta.

These three interpretations have been advanced to explain what is probably the same phenomenon. Somehow, a choice will have to be made among them.

The basement fault

The apparent time delay beyond 150 km can reasonably be explained by a normal fault striking across the profile with a downthrow of 5.6 km to the northwest. The good alignment of the delayed P_g branch with wide angle reflections from the Moho is taken as evidence that the down-fault depth remains relatively constant at least as far north as TAB. The calculated down-fault depth is 12.1 km, but the error could be as much as 1 km due to the inherent error of the calculations and the choice of an upper crustal velocity. Slightly north and east of this proposed fault, Chandra and Cumming (1972) have mapped the surface of the 6.5 km/s layer at approximately 12 km. They have also extrapolated this surface beneath the Trench at a depth of about 20 km. However, the evidence for this is not conclusive in their data. Price and Mountjoy (1970) calculated the depth to basement as 11 km beneath the Trench north of Golden. This was estimated by extrapolating from a depth calculation at the B.C. - Alberta border (from formation thicknesses in the thrust sheets) and a drill hole to the east.

If it is assumed that the last up-fault P_g arrival appears between 145 - 155 km, then the fault must be located at a distance of 133 - 143 km from the Kaiser shot point. On the map this zone occurs slightly south and to the east of Radium, extending several kilometers to the northwest. Although this fault has no obvious surface geologic expression near Radium, this may only reflect its Precambrian nature. Later tectonic activity would have been superimposed over a pre-existing fault; the decollement zone of thrusting lay along the basement surface and did not involve basement rocks (Bally et al, 1966).

From gravity and magnetic data, the strike of this fault appears to be northeasterly. In this region contours on the Bouguer gravity anomaly map show a pronounced change in strike to the northeast from the regional northwest trend; anomaly values decrease to the northwest, implying a decrease in density (Figure 16). Patterns on the residual total magnetic field map (Figure 17) also show northeasterly trends in

Figure 16. Bouguer gravity anomaly map of the Southern Rocky Mountains.
The outline of the Trench is indicated by the dashed lines.

Contour interval: 10 milligals   Scale: 1:5,000,000

(produced by the Observatories Branch,
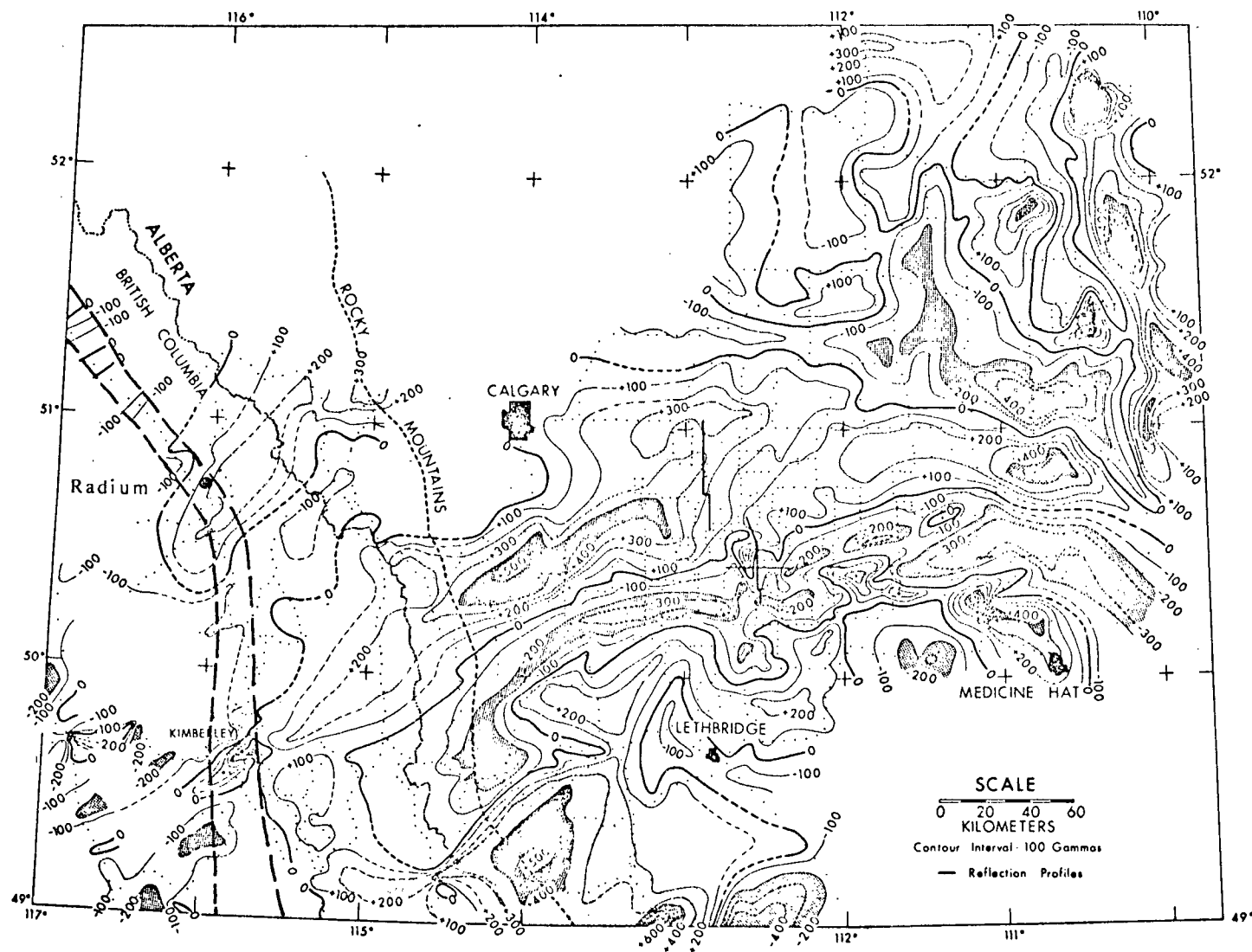Department of Energy, Mines & Resources, 1969)

Figure 17. Residual total magnetic field map for southern Alberta and southeastern British Columbia (Kanasewich et al., 1969). Outline of the Trench is indicated by the dashed lines.

the vicinity of 51°N, 116°W. A decrease from +200 gammas to -100 gammas seems to correlate with the zone of time delay seen in the seismic data. This same diagram shows the marked rift feature of Kanasewich et al (1969) to the south, a northeasterly trending zone characterized by a low of -300 gammas. In further support of this strike direction, northeasterly trending lineaments have been widely recognized in the Precambrian Shield of western Canada (Burwash, 1965).

Possible significance of the fault with respect to Trench origin

There is one significant alternative interpretation involving a basement fault. Figure 1 shows that the ray path from Kaiser intersects the Trench in precisely the same area over which the time delay is observed. Could this mean that the basement underlying the Rockies actually "disappears" beneath the Trench? If the Trench is an ancient zone of weakness, could not the basement and overlying rocks have been so deformed as to disguise an original smooth surface?

Of all the theories of Trench origin, the idea of a zone of weakness has held the most appeal. Daly (1912) first wondered if there was a genetic connection between the Trench and an ancient shore-line. Walker (1926) and Evans (1933) liked the idea, postulating that "a zone of weakness would exist in the basement rocks that might be reflected during the compression of later times." Both Henderson (1959) and Thompson (1962) believed that the zone of faulting along the Trench was related to the margin of an ancient continent, and that it marked the eastern hinge-line of the Cordilleran geosyncline. Leech (1964, 1965) argued for a fundamental basement control hypothesis – perhaps Mesozoic transcurrent faults, related to the cratonic boundary, have reasserted themselves through the fractured upper crust transported to the east above them. Although there is no evidence for Cenozoic strike-slip movement along the Trench, Roddick (1967) and Tempelman-Kluit (1972) have described extensive Cretaceous transcurrent faulting along the Tintina Trench to the north (Figure 1). Berry et al (1971) suggest that movement along these two faults may have been related; Souther (1970), Monger et al (1972) and Gabrielse (1972) find considerable evidence for transcurrent movement throughout the Cordillera before the mid-Jurassic period. Geophysical evidence that the Trench actually does mark the western edge of the craton was stated earlier and has been synthesized

by Berry et al (1971). They also make the point that the present thermal disturbance may have reactivated this old zone of weakness between crustal blocks. And finally, in a study of world-wide "geomagnetic variation anomalies", among which the Trench is included, Law and Riddihough (1971) have observed that all of them are related to plate margins.

All of this supports the idea that the basement rocks of the Trench were reworked over a long period of time, eliminating any sharp discontinuities which may have been present originally. The lack of a reflection from the Trench basement in the data of Bally et al (1966) could also be taken as supporting evidence for this theory. Even the most recent orogenic episode in the Rocky Mountains was characterized by alternate compression (thrusting) and tension (normal faulting) (e.g. Mudge, 1970). If future geophysical studies indicate that evidence for a normal fault striking across the Trench is meagre, then this can only mean strong support for this theory of Trench origin.

Crustal thickness

The validity of the crustal models naturally depends to a great extent on the lower crustal velocity and the presence of dip on the Moho, which cannot be detected by an unreversed profile. The selection of 6.5 km/s as the P_g velocity is unambiguous. It certainly cannot be any less, although it could be as high as 6.6 km/s. The constraint provided by the branch of reflections from the Moho is also unambiguous. It forces the inclusion of the velocity gradient seen in Figures 10, 12a, 13a, and 14a, resulting in an average lower crustal velocity of 6.8 km/s. Although no evidence for a deeper crustal layer was found in this data, Chandra and Cumming (1972) included a 7.15 km/s layer at a depth of 31 km under the foothills. Since the crustal structure beneath the Trench appears to be related to that found further to the east, the seemingly high average velocity of 6.8 km/s is quite reasonable. The question of dip on the Moho (and the basement) cannot be resolved, but the Bouguer gravity anomaly contours in Figure 16 suggest relative flatness along the profile. Also, the P_n velocity of 8.20 km/s obtained beneath the Trench by Chandra and Cumming (1972) agrees well with the observed value of 8.22 ± 0.04 km/s observed in this study.

Since the apparent velocities in the profile appear to be
close to the true velocities, the existence of a thick crust is
strongly suggested. Previous extrapolations have all indicated a
depth of less than 50 km (Chandra and Cumming, 1972; D.A. Forsyth,
oral communication, 1973). But even the low velocity zone model
gives a depth to the Moho of 56 km. If a deep crustal layer of
higher velocity were to be included, this value would be even greater.
The models calculated for a basement fault give a crustal thickness
to the northwest of 61 km or 58 km, depending on whether or not the
Moho is faulted. Up-fault, the corresponding depths are 61 km and
51 - 52 km. Owing to the inaccuracies of the calculations, these
depths may be in error by as much as 2 km.

Gravity models by Stacey (1973) for a profile across the
Cordillera from 49°N to 51°N have a crustal thickness of 60 km
beneath the Rocky Mountains. Therefore, as explained earlier, the
density change which he assumed to occur beneath the Trench does not
have to be moved to the east. This also agrees with the discovery
that the upper crustal velocity beneath the Trench is similar to that
found in the east. Price and Mountjoy (1970) claim that the total
thickness of the crust has been increased by at least 8 km due to the
accretion at the top which occurred in conjunction with the stacking
of thrust sheets. The Grenville Front, a similar long boundary
between two different geologic provinces, also exhibits a relative
thickening of the crust (Berry and Fuchs, 1973). In a geomagnetic
depth-sounding profile across the Trench, Dragert (1973) also required
considerable crustal thickening. Finally, the Bouguer gravity anomaly
along the Trench between 51°N and 53°N is very low, in places less than
-210 mgal. Although quantitative modelling has not been performed,
this gravity mimimum provides additional evidence for a thick crust.

A final judgement regarding the Moho topography is not
really possible with this data alone. The structure shown in Figure 14a
is preferred since it is best supported by evidence in the data. Since
Kanasewich et al (1969) have obtained strong evidence for a fault
throughout the crustal section, it may be reasonable to assume a similar
phenomenon in a similar feature to the north. Consequently, the more
extreme crustal thickness of 61 km could be rejected in favour of the
more conservative structure of 51 km south of Radium and 58 km to the north.

However, if it is discovered that the large amplitudes on C13 and B4
are not related to the Moho, this interpretation will have to be revised.

Converted S phase

The results of this section should be viewed with a certain
amount of skepticism. What is definitely known about this late
branch at the north end of the profile is that it is a shear wave and
that it travels with a high apparent velocity of 5.6 km/s. Its inter-
pretation as an S_n converted phase is only tentative – it is assumed
to convert from P to S after striking some form of discontinuity along
the Moho, subsequently travelling along this interface as an S_n wave.
Also, an upwards dip on the Moho beyond DAI cannot be confirmed by
the weak P_n arrivals beyond THO. However, there are several interesting
phenomena which may relate to this phase.

One is that the gravity values at the north end of the profile
increase rapidly beyond about THO, whereas they are very flat over most
of the southern part of the profile. This could be evidence for a rapid
thinning of the crust in the northwest. It could also be evidence for a
crustal fault with downthrow to the south, perhaps indicating that the
Rocky Mountains between $51^{\circ}N$ and $53^{\circ}N$ have depressed the crust-mantle
boundary.

The previously mentioned results of Caner et al (1971) show a
change in direction of the geomagnetic transition zone anomaly somewhere
between THO and TAB. This change would occur within the lower crust and
upper mantle and may be related to the S-wave conversion at this depth.

Finally, the anomalous outcroppings of Proterozoic rocks between
DAI and THO may be indirectly related to the question. A suggestion has
been made (P. Simony, oral communication, 1972) that these rocks have
actually been derived from the crystalline basement. If this is so,
it would appear that the basement in this region has been much more active
than in other parts of the Trench. Thus, it could be an expression of
a more widespread disturbance at depth in the crust, a condition which
could cause the observed conversion.

CONCLUSION

A seismic refraction survey has been conducted in the southern Rocky Mountain Trench. Detailed attention to amplitude scale factors has produced a record section which shows a smooth variation of energy with distance. An analysis of this section has led to the following conclusions:

(1) A basement anomaly has been detected just south of $51^{\circ}N$, $116^{\circ}W$ near Radium. It has been interpreted as a normal fault with a downthrow of 5.6 ± 1 km to the northwest. Comparison with local gravity and magnetic trends and with known lineaments in the Precambrian Shield has led to the conclusion that this fault strikes northeasterly across the Trench.

(2) If more detailed studies do not confirm the existence of a normal fault striking across the Trench, the seismic data will then strongly support the theory that the Trench marks an old zone of weakness in the basement. By this interpretation, the basement could be down-faulted and/or strongly reworked west of the east wall of the Trench.

(3) A preferred interpretation has the fault extend throughout the entire crustal section with up- and down-fault structures as shown in Figure 14a. Up-fault, a 5.5 km/s layer extends with a gradient to a depth of 6.5 ± 1 km, below which lies a 6.5 km/s layer to the Moho at 51 ± 2 km. Down-fault, the corresponding depths are 12.1 ± 1 km and 58 ± 2 km. A velocity gradient above the Moho is necessary. The existence of such a thick crust is strongly suggested by other geophysical and geological studies.

(4) An interpretation based on a thick sub-basement low velocity zone was achieved but thought to be unrealistic. However, even this model gives a thick (55 ± 2 km) crustal section.

(5) An analysis of arrivals delayed from the P_n phase is consistent with an interpretation of a low velocity zone 7 km thick, 8 km beneath the Moho. Other explanations have been offered for these arrivals, and a choice will have to be made among them.

(6) Study of a converted S phase has led to the tentative conclusion that the Moho surface dips steeply to the southeast beyond $53^{\circ}N$. Although this conclusion is based on rather slim seismic evidence, it is supported by interesting gravity, magnetic and geologic

phenomena in the region.

This study has interpreted several features of the Rocky Mountain Trench seismic data, and pointed the way to later studies. A detailed gravity/magnetic/seismic survey along the Trench from $49^{\circ}N$ to $51^{\circ}N$ would obtain more data relevant to the basement anomaly discovered in this data. It would also serve to tie in the rift feature of Kanasewich et al (1969). Some gravity and magnetic data is already available.

The velocity-depth structure as determined in this thesis should be refined by a gravity interpretation along the entire profile. This may also help to clarify the theories of a faulted Moho at $51^{\circ}N$ and a steep, southeasterly dipping Moho beyond $53^{\circ}N$.

Finally, there is much more to be gleaned from the seismic data. A more detailed study of the motions in the P-wave data must be integrated with an interpretation of the extensive S-wave arrivals. When this is accomplished, a more complete understanding of this enigmatic valley will be obtained.

REFERENCES

Bally, A.W., P.L. Gordy, and G.A. Stewart. Structure, seismic data and orogenic evolution of Southern Canadian Rocky Mountains. *Bull. Can. Soc. Petrol. Geol.*, 14, 337-381, 1966.

Barr, K.G. Crustal refraction experiment: Yellowknife 1966. *J. Geophys. Res.*, 76, 1929-1947, 1971.

Berry, M.J., W.R. Jacoby, E.R. Niblett, and R.A. Stacey. A review of geophysical studies in the Canadian Cordillera. *Can. J. Earth Sci.*, 8, 788-801, 1971.

Berry, M.J., and K. Fuchs. Crustal structure of the Superior and Grenville Provinces of the Northeastern Canadian Shield. *Bull. Seism. Soc. Am.*, 13, 1393-1432, 1973.

Burwash, R.A. Basement Architecture of Western Canada. *Alta. Soc. Petrol. Geol. 15th Field Conference Guide Book*, 280-288, 1965.

Caner, B., D.R. Auld, H. Dragert, and P.A. Camfield. Geomagnetic depth-sounding and crustal structure in western Canada. *J. Geophys. Res.*, 76, 7181-7201, 1971.

Cerveny, V. On dynamic properties of reflected and head waves in the n-layered earth's crust. *Geop. J. Roy. Astr. Soc.*, 11, 139-147, 1966.

Cerveny, V., and R. Ravindra. Theory of Seismic Head Waves, 312 pp. University of Toronto Press, 1971.

Chandra, N.N., and G.L. Cumming. Seismic refraction studies in western Canada. *Can. J. Earth Sci.*, 9, 1099-1109, 1972.

Crickmay, C.H. The Rocky Mountain Trench: a problem. *Can. J. Earth Sci.*, 1, 184-205, 1964.

Cumming, G.L., and E.R. Kanasewich. Crustal structure in western Canada. *Project Vela Uniform, Final Report*, AFCRL-66-159, 1966.

Dahlstrom, C.D.A. Structural geology of the eastern margin of the Canadian Rocky Mountains. *Bull. Can. Soc. Petrol. Geol.*, 18, 332-406, 1970.

Daly, R.A. Geology of the North American Cordillera at the 49th parallel. *Geol. Surv. Can. Memoir 38*, Parts 1 and 11, 1912.

Daly, R.A. Geological reconnaissance between Golden and Kamloops, B.C. *Geol. Surv. Can. Memoir 68*, 1915.

Dawson, G.M. Physical and geological features of the Rocky Mountains. *Geol. Surv. Can. Ann. Rept.*, 1, Report B, 1886.

Dragert, H. Broad-band geomagnetic depth-sounding along an anomalous
profile in the Canadian Cordillera. Ph.D. thesis,
University of B.C., 1973.

Eardley, A.J. Late Cenozoic trenches of the Rocky Mountains. *Bull.*
Geol. Soc. Am., 58, 1176, 1947 (abstract).

Ellis, R.M., and R.D. Russell. Monitoring of seismic activity
during loading of Mica Reservoir. *Semi-annual technical*
report to U.S. Geological Survey, Contract No. 14-08-0001-
13067, December, 1972.

Evans, C.S. Brisco-Dogtooth Map Area, B.C. *Geol. Surv. Can. Summ.*
Rept., 1932, AII, 106-176, 1933.

Forsyth, D.A.G. A refraction survey across the Canadian Cordillera.
M.Sc. thesis, University of B.C., 1973.

Gabrielse, H. Sedimentary facies and Northern Rocky Mountain Trench.
Prog. with Abstr. "Faults, fractures, lineaments and related
mineralization in the Canadian Cordillera". Cordilleran Sect.
Geol. Assoc. Can. conference, Feb., 1972.

Garland, G.D., E.R. Kanasawich, and T.L. Thompson. Gravity measurements
over the southern Rocky Mountain Trench area of B.C. *J. Geo-*
phys. Res., 66, 2495-2505, 1961.

Haines, G.V., W. Hannaford, and R.P. Riddihough. Magnetic anomalies
over British Columbia and the adjacent Pacific Ocean.
Can. J. Earth Sci., 8, 387-391, 1971.

Hales, A.L., and J.B. Nation. A seismic refraction survey in the
Northern Rocky Mountains: More evidence for an intermediate
crustal layer. *Contribution No. 228, Inst. Geol. Sciences,*
University of Texas at Dallas, 1973 (in press).

Henderson, G.G.L. A summary of the regional structure and stratigraphy
of the Rocky Mountain Trench. *Can. Inst. Min. Metal. Bull.,*
52, 322-327, 1959.

Holland, S.S. Symposium on the Rocky Mountain Trench: Introduction.
Can. Inst. Min. Metal. Bull., 52, 318, 1959.

Jones, H.J., and J.A. Morrison. Cross-correlation filtering. *Geophysics*,
19, 660-683, 1954.

Kanasewich, E.R., R.M. Clowes, and C.H. McCloughan. A buried
precambrian rift in Western Canada. *Tecton.,*8, 513-527, 1969.

Kanasewich, E.R. Time Sequence Analysis in Geophysics, (pre-
publication manuscript), University of Alberta Press,
1974, (in press).

Kollar, F. and R.D. Russell. Seismometer analysis using an electric current analog. *Bull. Seism. Soc. Am.*, 56, 1193-1205, 1966.

Lamb, A.T. and D.W. Smith. Refraction profiles over the southern Rocky Mountain Trench area of B.C. *J. Alta. Soc. Petrol. Geol.*, 10, 428-437, 1962.

Law, L.K. and R.P. Riddihough. A geographical relation between geomagnetic variation anomalies and tectonics. *Can. J. Earth Sci.*, 8, 1094-1106, 1971.

Leech, G.B. The southern part of the Rocky Mountain Trench. *Can. Inst. Min. Metal. Bull.*, 52, 327-333, 1959.

Leech, G.B. Rocky Mountain Trench. *Geol. Soc. Am. Spec. Paper 76*, p. 100, 1964 (abstract).

Leech, G.B. The Rocky Mountain Trench, in The World Rift System, *Geol. Surv. Can. Paper 66-14*, 307-329, 1965.

Monger, J.W.H., J.G. Souther and H. Gabrielse. Evolution of the Canadian Cordillera: a plate-tectonic model. *Am. J. Sci.*, 272, 577-602, 1972.

Mudge, M.R. Origin of the disturbed belt in northwestern Montana. *Bull. Geol. Soc. Am.*, 81, 377-392, 1970.

Mueller, S. and M. Landisman. Seismic studies of the earth's crust in continents. Part I: Evidence for a low velocity zone in the upper part of the lithosphere. *Geop. J. Roy. Astr. Soc.*, 10, 525-538, 1966.

North, F.K. and G.G.L. Henderson. The Rocky Mountain Trench. *Alta. Soc. Petrol. Geol. 4th Annual Field Conference Guide Book*, 82-100, 1954.

Price, R.A. and E.W. Mountjoy. Geologic structure of the Canadian Rocky Mountains between Bow and Athabasca Rivers. *Geol. Assoc. Can. Spec. Paper No. 6*, 7-25, 1970.

Roddick, J.A. Tintina Trench. *J. Geol.*, 75, 23-33, 1967.

Schofield, S.J. The origin of the Rocky Mountain Trench, B.C. *Trans. Roy. Soc. Can.*, 3rd ser., 14, sec. 4, 61-97, 1921.

Shepard, F.P. The structural relation of the Purcell Range and the Rocky Mountains of Canada. *J. Geol.*, 30, 130-139, 1922.

Shepard, F.P. Further investigations of the Rocky Mountain Trench. *J. Geol.*, 34, 623-641, 1926.

Simony, P., H. Baer, E. Ghent, Y. Helfenbein, F. Meilliez and J. Terry. Structural detail in a portion of the southern Rocky Mountain Trench. *Prog. with Abstr. "Faults, fractures, lineaments and related mineralization in the Canadian Cordillera"*. Cordilleran Sect. Geol. Assoc. Can. conference, Feb., 1972.

Souther, J.G.   Volcanism and its relationship to recent crustal movements
        in the Canadian Cordillera.   *Can. J. Earth Sci.*, 7, 553-568, 1970.

Stacey, R.A.   Gravity anomalies, crustal structure and plate tectonics in
        the Canadian Cordillera.   *Can. J. Earth Sci.*, 10, 615-628, 1973.

Tempelman-Kluit, D.J.   Evidence for timing and magnitude of movement along
        Tintina Trench.   *Prog. with Abstr. "Faults, fractures, lineaments,
        and related mineralization in the Canadian Cordillera"*.
        Cordilleran Sect. Geol. Assoc. Can. conference, Feb., 1972.

Thompson, T.L.   Origin of the Rocky Mountain Trench in southern B.C. by
        Cenozoic block faulting.   *J. Alta. Soc. Petrol. Geol.*, 10,
        408-427, 1962.

Walker, J.F.   Geology and mineral deposits of Windermere map-area.
        Geol. Surv. Can. Memoir 148, 1926.

White, W.R.H., M.N. Bone and W.G. Milne.   Seismic refraction surveys in
        British Columbia – a preliminary interpretation.   *Am. Geophys.
        Un. Mono. No. 12*, 81-93, 1968.

Wiggins, R.A. and J.A. Madrid.   Body wave amplitude calculations.
   *submitted to Geop. J.*, 1974 (in press).

APPENDIX

Corrections for HRGLTZ Fault Models

In this procedure the following assumptions have been made:

(1) The equations of geometric ray theory are valid for the calculation of traveltimes.

(2) Average velocities can be used in layers containing velocity gradients.

(3) The fault throw is much less than the horizontal distance of the fault from the shot point.

(4) Seismic energy in the body wave incident upon the lower corner of the fault is partially converted into a head wave which continues along the downthrown surface.

1. Correction to P_g intercept time for a fault on the basement
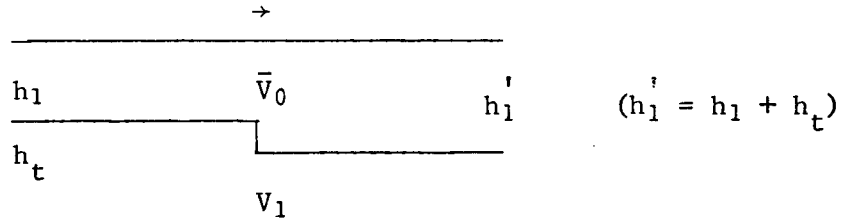
Denote the head wave intercept time by T and average velocities by $\bar{V}$.

$$T_1 = 2h_1 \sqrt{V_1^2 - \bar{V}_0^2} \, (\bar{V}_0 V_1)^{-1} \quad \text{for a model based on the up-fault structure}$$

$$T_1' = 2h_1' \sqrt{V_1^2 - \bar{V}_0^2} \, (\bar{V}_0 V_1)^{-1} \quad \text{for a model based on the down-fault structure}$$

If $\Delta\tau$ is the delay time in the data due to the fault, and ΔT is the time correction which must be added to the down-fault intercept in the data (i.e. a HRGLTZ model delayed by ΔT from the down-fault intercept will give the desired h_1' structure), then:

$$\Delta T = T_1' - (T_1 + \Delta\tau)$$

By assumptions (3) and (4) it can be shown that:

$$\Delta\tau = h_t V_1 (\bar{V}_0 \sqrt{V_1^2 - \bar{V}_0^2})^{-1}$$

Therefore,

$$\Delta T = 2(h_1' - h_1) \sqrt{V_1^2 - \bar{V}_0^2} \ (\bar{V}_0 V_1)^{-1} - \Delta\tau$$

$$= 2\Delta\tau(V_1^2 - \bar{V}_0^2) \ (V_1)^{-2} - \Delta\tau$$

$$\Delta T = \Delta\tau(V_1^2 - 2\bar{V}_0^2)/V_1^2$$

In the seismic data,

$$\Delta\tau = 1.7 \ \text{sec}$$
$$V_1 = 6.5 \ \text{km/s}$$
$$\bar{V}_0 = 5.7 \ \text{km/s}$$

$$\rightarrow \quad \Delta T = -0.89 \ \text{sec}$$

The value of the average upper crustal velocity was repeatedly checked during the modelling to ensure its accuracy. Therefore, a HRGLTZ model was produced such that its P_g intercept was earlier than the down-fault P_g intercept in the data by 0.89 sec. This gave $h_1' = 12.1$ km. Knowing that $h_1 = 6.5$ km from the up-fault model, a throw of $h_t = 5.6$ km was calculated for the basement fault.

2.0 General correction to P_n intercept time for faults on the basement and Moho
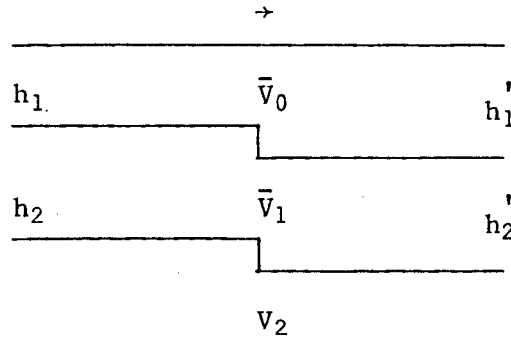
Let h_{1_t} and h_{2_t} be the fault throws at the basement and Moho surfaces, respectively.

$$T_2 = 2h_1\sqrt{V_2^2 - \bar{V}_0^2} \ /V_2\bar{V}_0 + 2h_2\sqrt{V_2^2 - \bar{V}_1^2} \ /V_2\bar{V}_1$$

for a model based on the up-fault structure

$$T_2' = 2h_1'\sqrt{V_2^2 - \bar{\bar{V}}_0^2}\,/V_2\bar{V}_0 + 2h_2'\sqrt{V_2^2 - \bar{V}_1^2}\,/V_2\bar{V}_1$$

for a model based on the down-fault structure

Let $\Delta\tau_1$ be the delay time in the data due to the action of the basement fault (this is a second order effect only) and $\Delta\tau_2$ be the delay time in the data due to the action of the Moho fault. Therefore:

$$\Delta T = T_2' - (T_2 + \Delta\tau_1 + \Delta\tau_2)$$

As in Section 1, it can be shown that:

$$\Delta\tau_2 = h_{2_t}V_2\,(\bar{V}_1\sqrt{V_2^2 - \bar{V}_1^2}\,)^{-1}$$

It can also be shown that:

$$\Delta\tau_1 = h_{1_t}V_2\{(\bar{V}_0\sqrt{V_2^2 - \bar{V}_0^2}\,)^{-1} - (V_1\sqrt{V_2^2 - V_1^2}\,)^{-1}\}$$

Therefore, it follows that:

$$\Delta T = 2h_{1_t}\sqrt{V_2^2 - \bar{V}_0^2}\,/V_2\bar{V}_0 + 2(h_2' - h_2)\sqrt{V_2^2 - \bar{V}_1^2}\,/V_2\bar{V}_1$$
$$- h_{1_t}V_2\{(\bar{V}_0\sqrt{V_2^2 - \bar{V}_0^2}\,)^{-1} - (V_1\sqrt{V_2^2 - V_1^2}\,)^{-1}\}$$
$$- h_{2_t}V_2\,(\bar{V}_1\sqrt{V_2^2 - \bar{V}_1^2}\,)^{-1}$$

This result will be applied in the following sections.

2.1 Faulted basement, unfaulted Moho (Figures 12a and 12b)

$$h_{2_t} = 0 \qquad \text{and} \qquad h_2' - h_2 = -h_{1_t}$$

$$\Delta T = 2h_{1_t}\{(\sqrt{V_2^2 - \bar{V}_0^2}\,/\bar{V}_0) - (\sqrt{V_2^2 - \bar{V}_1^2}\,/\bar{V}_1)\}/V_2$$
$$- h_{1_t}V_2\{(\bar{V}_0\sqrt{V_2^2 - \bar{V}_0^2}\,)^{-1} - (V_1\sqrt{V_2^2 - V_1^2}\,)^{-1}\}$$

In the seismic data,

$$V_2 = 8.2 \text{ km/s}$$
$$\bar{V}_1 = 6.8 \text{ km/s}$$
$$V_1 = 6.5 \text{ km/s}$$
$$\bar{V}_0 = 5.7 \text{ km/s}$$

From the calculations in Section 1, h_{1_t} = 5.6 km.

Therefore:

ΔT = 0.54 sec

As in Section 1, the value of the average lower crustal velocity was repeatedly checked during the modelling to ensure its accuracy. Therefore, a HRGLTZ model was produced such that its P_n intercept was delayed from the P_n intercept in the data by 0.54 sec. The resulting model gives a crustal thickness of $(h_1' + h_2') = 61.2$ km before and after the basement fault.

2.2 Constant fault throw throughout the crustal section (Figures 13a and 13b)

$$h_{1_t} = h_{2_t} \qquad \text{and} \qquad h_2' - h_2 = 0$$

$$\Delta T = 2h_{1_t}(\sqrt{V_2{}^2 - \bar{V}_0{}^2}/\bar{V}_0)/V_2 - h_{1_t}V_2\{(\bar{V}_0\sqrt{V_2{}^2 - \bar{V}_0{}^2})^{-1}$$

$$- (V_1\sqrt{V_2{}^2 - V_1{}^2})^{-1} + (\bar{V}_1\sqrt{V_2{}^2 - \bar{V}_1{}^2})^{-1}\}$$

For the same data parameters as Section 2.1:

ΔT = -0.01 sec

Therefore, a HRGLTZ model was produced such that its P_n intercept was earlier than the P_n intercept in the data by 0.01 sec. The resulting model gives a down-fault crustal thickness of $(h_1' + h_2') = 57.8$ km. Since the fault throw is assumed to be constant throught the crustal section, the up-fault crustal thickness is then $(h_1' + h_2' - h_{1_t}) = 52.2$ km.

2.3 Fault throw calculated from the pre-fault P_n intercept

$$h_2' - h_2 = h_{2_t} - h_{1_t} \qquad \text{and } \Delta\tau_2 \text{ is picked from the data}$$

$$\Delta T = 2h_{1_t}\{(\sqrt{V_2{}^2 - \bar{V}_0{}^2}/\bar{V}_0) - (\sqrt{V_2{}^2 - \bar{V}_1{}^2}/\bar{V}_1)\}/V_2$$

$$-h_{1_t}V_2\{(\bar{V}_0\sqrt{V_2{}^2 - \bar{V}_0{}^2})^{-1} - (V_1\sqrt{V_2{}^2 - V_1{}^2})^{-1}\}$$

$$-\Delta\tau_2\{(2\bar{V}_1{}^2/V_2{}^2) - 1\}$$

Using the same data parameters as Section 2.1, and in addition:

$\Delta\tau_2 = 1.5$ sec

$\Delta T = -0.04$ sec

Therefore, a HRGLTZ model was produced such that its P_n intercept was earlier than the P_n intercept in the data by 0.04 sec. The resulting structure gave a down-fault crustal thickness $(h_1' + h_2') = 57.6$ km. A HRGLTZ model was then run for the up-fault model such that its P_n intercept was delayed from the P_n intercept in the data (the up-fault intercept given by the phase on C13 and B4) by an amount $\Delta\tau_1$ due to the extra thickness of the down-fault upper crustal layer. From the above calculations, $\Delta\tau_1 = -0.05$ sec, therefore the HRGLTZ intercept was early by 0.05 sec. The resulting model gave an upfault crustal thickness of $(h_1 + h_2) = 50.8$ km. Therefore, the fault throw on the Moho is $h_{2_t} = 6.8$ km.